Nucleic Acids Research, 2024, **52**, 3702–3721
https://doi.org/10.1093/nar/gkae157
Advance access publication date: 28 February 2024
Gene regulation, Chromatin and Epigenetics

A circular RNA-gawky-chromatin regulatory axis modulates stress-induced transcription

Rui Su[1,†], Min Zhou[2,3,†], Jiamei Lin[1,†], Ge Shan[4] and Chuan Huang[1,*]

[1]School of Life Sciences, Chongqing University, Chongqing 401331, China
[2]Department of Obstetrics and Gynecology, Women and Children's Hospital of Chongqing Medical University, Chongqing 401147, China
[3]Department of Obstetrics and Gynecology, Chongqing Health Center for Women and Children, Chongqing 401147, China
[4]School of Basic Medical Sciences, Division of Life Science and Medicine, University of Science and Technology of China, Hefei 230027, China

[*]To whom correspondence should be addressed. Tel: +86 19956025374; Email: chuanhuang@cqu.edu.cn
[†]The first three authors should be regarded as Joint First Authors.

Abstract

In response to heavy metal stress, the RNA-binding protein (RBP) gawky translocates into the nucleus and acts as a chromatin-interacting factor to activate the transcription of many stress-responsive genes. However, the upstream regulators of gawky-mediated transcription and their mechanistic details remain unknown. Here, we identified a class of metal-responsive element-containing circRNAs (MRE circRNAs) which specifically interact with gawky during copper stress. Using classic stress-responsive genes as a readout (*Drosophila MT*), we found that overexpression of MRE circRNAs led to a significant repression in stress-induced transcription. Mechanistically, MRE circRNAs promote the dissociation of gawky from chromatin and increase its aberrant cytoplasmic accumulation, which ultimately impedes the loading of RNA polymerase II to the active gene loci. The MRE motif serves as an important RNA regulon for maintaining the circRNA–gawky interaction, loss of which impaired the inhibitory effects of MRE circRNAs on gawky. Through RNA-seq analyses, we then identified over 500 additional stress-responsive genes whose induced transcription was attenuated upon MRE circRNA overexpression. Finally, we uncovered the physiological relevance of MRE circRNA-mediated regulation in cellular defense against copper overloading. Taken together, this study proposes that the circRNA-RBP-chromatin axis may represent a fundamental regulatory network for gene expression in eukaryotic cells.

Graphical abstract

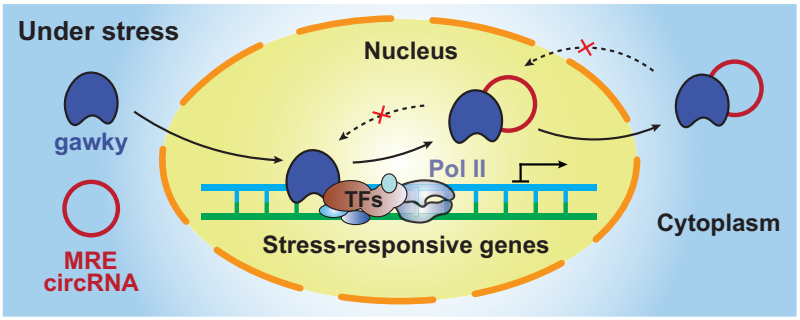

Introduction

To guard against dramatic and adverse changes in the environmental conditions, cells immediately make a series of adaptive responses to minimize intracellular perturbations and eventually increase cell survival (reviewed in (1,2)). Particularly, the adjustment of RNA synthesis through the transcriptional reprogramming of stress-responsive genes is a major component among these adaptive responses (reviewed in (1,2)). In fact, stress-induced transcription is a complex process which is tightly regulated by RNA polymerase II (Pol II), transcription factors (TFs) and even RNA-binding proteins (RBPs) (reviewed in (1–4)). Elucidating the molecular details of stress-induced transcription may provide us a deeper understanding of the dynamic coordination of transcription programmes.

RBPs represent a huge repertoire of more than 2000 proteins that have a capacity to directly interact with a variety of RNA species via one or multiple RNA-binding domains (reviewed in (5–7)). RBPs were long thought as a type of crucial post-transcriptional modulators involved in nearly every step of the RNA life span, including splicing, modification, nuclear export, translation and degradation (reviewed in (5–7)). For example, the RNA helicase UPF1 can recognize the base-paired structures within the 3′ untranslated region (UTR) of mRNAs, and then recruits mRNAs to its interacting endoribonuclease G3BP1 for efficient degradation (8).

Received: November 22, 2023. **Revised:** February 14, 2024. **Editorial Decision:** February 18, 2024. **Accepted:** February 20, 2024

Of note, a subset of RBPs were recently found to accumulate in open chromatin regions, such as enhancers and promoters (9–15). In addition, emerging studies have revealed the non-canonical and underestimated functions of these chromatin-interacting RBPs (ChRBPs) in the process of transcription regulation (9–15), broadening the functional diversity of RBPs. For example, the ChRBP PSPC1 harbors a high content of intrinsically disordered regions at its C-terminus (up to 66%) and functions as a central organizer by gathering Pol II, the TATA-box binding protein TBP and nascent short transcripts together to stimulate the formation of phase-separated condensates within the active genome positions, thereby ensuring a stable Pol II-DNA engagement as well as continuous transcription (9). In regard to the transcription of stress-responsive genes, we previously demonstrated that the ChRBPs Hlc and gawky function as essential regulators in basal and stress-induced transcription, respectively, through distinct mechanisms (10,11). Under normal conditions, Hlc sustains the basal transcription of stress-responsive genes by maintaining an open and accessible chromatin architecture adjacent to the transcriptional start sites (TSSs) (10). In response to heavy metal stress, gawky rapidly moves into the nucleus and recruits the metal-activated TF MTF-1 to the promoters of stress-responsive genes, which ultimately assists the loading of Pol II and additional TFs for efficient initiation of stress-induced transcription (11). More interestingly, the negative cooperativity between Hlc and gawky on chromatin during the transition from normal to stressed conditions indicates that these ChRBPs are key 'checkpoints' in discrimination of the two transcription states (10,11). It is also important to point out that most ChRBPs identified so far cannot stay permanently bound to chromatin. Instead, the ChRBP-chromatin interaction is often transient and usually occurs under specific conditions (10–15). We therefore make a deduction that the dynamic changes in the interaction require sophisticated mechanisms and are fundamental for the proper regulatory activities of ChRBPs. However, the upstream regulators of ChRBPs and their mechanistic nature remain challenging and outstanding questions.

As a category of single-stranded and covalently-closed transcripts, circular RNAs (circRNAs) are common and pervasive outputs generated from thousands of eukaryotic protein-coding genes via back-splicing, a reaction during which a downstream splicing site is connected to an upstream one (reviewed in (16–20)). Despite being considered as junk transcripts over the years, many circRNAs have been recently uncovered to have crucial roles in various molecular and physiological events through diverse mechanisms, such as sponging miRNAs, acting as protein scaffolds/decoys and even translating into functional proteins (reviewed in (21–25)). For example, a *Drosophila sfl* derived circRNA can make use of an AUG start codon same to its linear counterpart and a TAA in-frame stop codon after the back-splicing junction (BSJ) (26), and its encoded product (a ∼25 kDa truncated sfl protein) is capable of enhancing cellular resistance to heat stress (27) as well as prolonging the lifespan of fruit flies (26). In particular, the functions of circRNAs in the nucleus are coming into focus in recent years (28–33). A case in point is *circSEPALLATA3* which can induce an exon-skipping event of its host linear mRNA by forming a stable RNA–DNA hybrid (also known as R-loop) at the sixth exon of the *SEPALLATA3* locus (30). Due to the structure feature of circRNAs, they are resistant to degradation by exonucleases and their half-lives are much longer than those of linear transcripts (34–36). Therefore, we reason that circRNAs may represent stable and potent modulators in fine-tuning the distributions and functional activities of ChRBPs on chromatin. Nevertheless, the assumption remains yet to be defined and the related studies are still very limited.

Concentrating on the ChRBP gawky-mediated transcription in this study, we identified a class of gawky-interacting circRNAs which comprise a sequence motif called metal-responsive element (MRE). These circRNAs, termed MRE circRNAs herein, are stress-responsive molecules with distinct nuclear-cytoplasmic distributions under normal and copper-stressed conditions. Focused investigations on *circCG32369(2)* and *circMCPH1(2,3,4,5)*, two representative MRE circRNAs, revealed that they act as potent negative regulators for dictating stress-induced transcription. Mechanistically, MRE circRNAs can inhibit the functional activity of gawky by antagonizing gawky recruitment to active chromatin regions and inducing its aberrant cytoplasmic accumulation. Importantly, the MRE motif within circRNAs was identified as a necessary RNA regulon for sustaining the circRNA-gawky interaction, which is indispensable for the inhibitory effects of MRE circRNAs on stress-induced transcription. Using RNA-seq, we further corroborated that MRE circRNA-meditated transcription repression represents a widespread mechanism for hundreds of stress-responsive genes in *Drosophila*. Moreover, we found that MRE circRNAs can aggravate copper-induced DNA damage and reduce cellular resistance to copper stress, suggesting a new pathway to remove damaged cells in response to stressed conditions. Altogether, the unexpected functional relevance between MRE circRNAs and the ChRBP gawky in orchestrating transcription provides novel insights into the molecular basis of gene expression regulation beyond the canonical regulatory steps.

Materials and methods

Cell culture

Drosophila Schneider 2 (S2) cells were cultured in Schneider's *Drosophila* medium (SDM, Sigma, S9895) with 10% (v/v) fetal bovine serum (FBS, Excell Bio, FSP500) and 1% (v/v) penicillin-streptomycin (Biosharp, BL505A) at 25°C. To activate copper-induced transcription (if applicable), cells were treated with 500 μM copper sulfate for the indicated amounts of time before harvest.

RNA interference (RNAi)

To knock down the indicated MRE circRNA, a total of 0.8×10^6 cells were transfected with the BSJ-targeting siRNA (final concentration: 80 nM) using LipoRNAi™ (Beyotime, C0535) according to the manufacturer's protocol, and cells were then cultured for 2 days at 25°C before harvest. To knock down the indicated protein-coding gene (gawky, Hlc or β-gal), 8 μg of double-strand RNA (dsRNA) was added into 600 μl of serum-free SDM containing 1.5×10^6 cells for 30 min at room temperature. Afterwards, 400 μl of SDM with 20% (v/v) FBS was added, and cells were cultured for 3 days at 25°C before harvest. For dsRNA preparation, DNA templates were first amplified through the polymerase chain reaction (PCR) using PrimeSTAR® Max DNA Polymerase (Takara, R045) with primers harboring the T7 promoter sequence (TAATACGACTCACTATAGGG) upstream of their 5′ ends. DsRNAs

were then produced by the *in vitro* transcription assay using ScriptMAX® Thermo T7 Transcription Kit (TOYOBO, TSK-101). The detailed information of siRNAs and dsRNAs used in this study is provided in Supplementary Table S1.

Vectors, cloning and stable cell line construction

Vectors for overexpressing circRNAs were constructed by inserting the circularizing sequences into the multiple cloning site (MCS) of the Hy_pAct5C laccase2 MCS exon vector (modified from (27,37); Supplementary Plasmid Information). Vectors for overexpressing linear RNAs were constructed by inserting the indicated sequences into the MCS of the Hy_pAct5C MCS vector (modified from (11,27); Supplementary Plasmid Information). To generate a stable cell line, S2 cells were transfected with the indicated overexpression vector using Lipo6000™ (Beyotime, C0526) according to the manufacturer's protocol, and then maintained in SDM containing 150 μg/ml hygromycin B (BioFroxx, 1366ML010) for 3–5 weeks.

RNA purification, reverse transcription and quantitative PCR (RT-qPCR)

RNA extracts were purified using RNAiso Plus (Takara, 9109). Complementary DNAs (cDNAs) were synthesized from 500 ng of RNA by the reverse transcription assay using PrimeScript RT Master Mix (Takara, RR036A) according to the manufacturer's protocol. QPCR was performed using 2 × Universal SYBR Green Fast qPCR Mix (ABclonal, RK21203) with the CFX connect real-time PCR system (Bio-Rad). The MIQE (minimum information for publication of qPCR experiments) checklist and primer sequences are provided in Supplementary Table S2 and S3, respectively. Quantitative analysis of RNA copy number was performed as previously described (28). In brief, double-stranded DNA (dsDNA) fragments corresponding to MRE circRNAs were amplified by PCR with cDNAs and individually inserted into the pUCm-T vectors (Beyotime, D2006) according to the manufacturer's protocol. A series of dilutions of the recombinant vectors were then applied to plot a standard curve by qPCR assays. The copies of MRE circRNAs per cell were calculated based on the numbers of cells used for quantification and the Ct values from RT-qPCR assays.

Nucleocytoplasmic separation

Subcellular fractionation was performed to assess the nuclear-cytoplasmic distributions of MRE circRNAs and their linear counterparts. Briefly, cells were washed with 1 × phosphate buffer saline (PBS, pH 7.4: 137 mM NaCl, 2.7 mM KCl, 10 mM Na_2HPO_4 and 1.8 mM KH_2PO_4) for 2–3 times and resuspended with slow pipetting into 1 ml of ice-cold RLN1 buffer (50 mM Tris–HCl pH 8, 140 mM NaCl, 1.5 mM $MgCl_2$ and 0.5% (v/v) NP40). After being incubated on ice for 5 min, the sample was centrifuged at 300 × g for 5 min at 4°C. The supernatant, as the cytoplasmic fraction, was collected and centrifuged at 13 000 × g for 5 min at 4°C to remove debris. The initial pellet was gently resuspended into 500 μl of ice-cold RLN1 buffer and centrifuged at 1000 × g for 5 min at 4°C to remove cytoplasmic contamination. The final pellet was resuspended into 225 μl of ice-cold RLN2 buffer (50 mM Tris–HCl pH 8, 500 mM NaCl, 1.5 mM $MgCl_2$ and 0.5% (v/v) NP40) and saved as the nuclear fraction. Subsequently, nuclear and cytoplasmic RNAs were purified using RNAiso Plus (Takara, 9109) and subjected to circRNA-seq or RT-qPCR assays. Purity of subcellular fractionation was confirmed by RT-qPCR using nuclear (*U6*) and cytoplasmic (*Act42A*) markers.

Protein extraction and western blotting

For protein extraction from whole-cell samples, cells were washed with 1ml of 1 × PBS buffer for 3 times, resuspended into 70 μl of RIPA buffer (50 mM Tris–HCl pH 7.4, 150 mM NaCl, 0.1% (w/v) sodium dodecyl sulfate (SDS), 1% (w/v) sodium deoxycholate and 1% (v/v) Triton X-100), placed on ice for 40 min and vigorously pipetted for 100 rounds. The sample was centrifuged at 13 000 × g for 5 min at 4°C to remove debris and collected as protein extracts. Proteins were denatured at 100°C for 5 min with protein loading buffer (62.5 mM Tris–HCl pH 6.8, 10% (v/v) glycerol, 0.01% (w/v) bromophenol blue, 2.15% (w/v) SDS, 1.55% (w/v) dithiothreitol and 5% (v/v) 2-hydroxy-1-ethanethiol), separated through SDS-polyacrylamide gel electrophoresis and then transferred to polyvinylidene fluoride (PVDF) membranes (Merck Millipore, IPVH00010). Membranes were treated with 5% (w/v) skim milk (BioFroxx, 1172GR100) in TBST buffer (Tris-buffered saline Tween-20 pH 7.6: 0.242% (w/v) Tris–HCl, 0.8% (w/v) NaCl and 0.05% (v/v) Tween-20) for 30 min at room temperature and incubated with the indicated primary antibody at 4°C overnight. After being washed with TBST buffer for 3 times, membranes were incubated with the horseradish peroxidase (HRP)-labeled secondary antibody for 2 h at room temperature and viewed using BeyoECL Plus (Beyotime, P0018S) with the Bio-Rad ChemiDoc Imaging System. These antibodies were utilized in western blotting assays: anti-FLAG (Beyotime, AF519; 1:1000), anti-α-Tubulin (Beyotime, AT819; 1:2000), anti-Histone H3 (Abcam, ab1791; 1:1000), anti-gawky (previously described in (11); 1:250), anti-Hlc (previously described in (10); 1:1000), HRP-labeled goat anti-mouse IgG (H + L) (Beyotime, A0216; 1:10 000) and HRP-labeled goat anti-rabbit IgG (H + L) (Beyotime, A0208; 1:10 000).

Immunofluorescence staining

Immunofluorescence staining was used to examine the nuclear-cytoplasmic distribution of gawky as well as the level of DNA damage. Since S2 cells are a type of semi-adherent cells, coverslips for fluorescence imaging were coated with concanavalin A (Con A; Solarbio, C8110) to increase cell attachment before use. A total of 1.0×10^5 cells were seeded onto a ConA-coated coverslip in a well of a 6-well plate for 2 h. Then coverslips (cell side up) were washed with 1 × PBS buffer for 2–3 times, incubated with fixative solution (75% (v/v) methanol and 25% (v/v) glacial acetic acid) for 10 min and treated with 0.1% Triton X-100 in TBST buffer to permeabilize cells for 5 min. To avoid non-specific binding of antibodies, cells were incubated with 5% (w/v) bovine serum albumin (BSA, Beyotime, ST025) in TBST buffer for 1 hr at room temperature. After incubation with the indicated primary antibody for 12 h at 4°C, coverslips were incubated with the fluorescent secondary antibody at room temperature for 2 h in the dark. Fluorescence signals were captured with a Leica confocal system (TCS SP8 DIVE) and analyzed using the ImageJ software. These antibodies were utilized in immunofluorescence staining assays: anti-γH2A.V (Beyotime, AF1201; 1:200), anti-gawky (previously described in (11); 1:50) and

Alexa Fluor 488-labeled goat anti-rabbit IgG (H + L) (Beyotime, A0423; 1:100).

Fluorescence *in situ* hybridization (FISH)

Fluorescent RNA probes were produced by *in vitro* transcription using ScriptMAX® Thermo T7 Transcription Kit (TOYOBO, TSK-101) and labeled with the Alexa Fluor 488 or 546 dye using ULYSIS Nucleic Acid Labeling Kit (Invitrogen, U21650 and U21652). The probe sequences are listed in Supplementary Table S4. FISH was performed as previously described (10,11,27) and used to examine the nuclear-cytoplasmic distributions of *circCG32369(2)* and *circpxb(3,4)* as well as the expression levels of *MtnA*, *MtnB* and *Act42A*. Briefly, after being seeded onto a ConA-coated coverslip for 2 hr, cells were fixed by fixative solution (75% (v/v) methanol and 25% (v/v) glacial acetic acid) for 10 min, washed with 0.5% (v/v) Tween 20 in 2 × SSC buffer (saline sodium citrate pH 7.0: 300 mM NaCl and 30 mM sodium citrate) twice and permeabilized with 0.1% (v/v) Triton X-100 in 2 × SSC buffer for 10 min. Afterwards, cells were denatured at 80°C for 10 min, incubated with 10–100 ng of denatured RNA probes at 42°C overnight, washed with 0.5% (v/v) Tween 20 in 2 × SSC buffer twice to remove uncombined probes and stained with 1μg/ml DAPI (Beyotime, C1002) for 5 min before imaging. Fluorescence signals were detected with a Leica confocal system (TCS SP8 DIVE) and analyzed using the ImageJ software.

Chromatin immunoprecipitation (ChIP)

ChIP was conducted using ChIP Assay Kit (Beyotime, P2078) according to the manufacturer's protocol and used to evaluate the binding of gawky, Hlc, Pol II or MTF-1 to the genomic *MtnB*. Cells were resuspended into 1 × PBS buffer containing 1 mM phenylmethanesulfonyl fluoride (PMSF, a protease inhibitor), cross-linked with 1% (v/v) formaldehyde at 37°C for 10 min and treated with glycine (final concentration: 125 mM) at room temperature for 5 min to terminate the cross-linking reaction. After centrifugation at 500 × g for 5 min, fixed cells were resuspended into ice-cold SDS lysis buffer (50 mM Tris–HCl pH 8.1, 1% (w/v) SDS, 10 mM EDTA and 1 mM PMSF) with 10–20 rounds of vigorous pipetting and sonicated on ice using an ultrasonic cell disruptor (Scientz-IID Sonicator) to yield chromatin solution consisting of genomic DNA fragments between 100–500 bp. The fragment mix was centrifuged at 12 000 × g at 4°C for 5 min to remove cell debris and diluted (1:10) into ChIP dilution buffer (16.7 mM Tris–HCl pH 8.1, 167 mM NaCl, 0.01% (w/v) SDS, 1.1% (v/v) Triton X-100, 1.2 mM EDTA and 1 mM PMSF). Using Protein A + G Agarose beads (Beyotime, P2055-50), the mix was then precleared and immunoprecipitated with anti-gawky (previously described in (11)), anti-Hlc (previously described in (10)), anti-Pol II (Abcam, ab5095) and anti-MTF-1 (previously described in (11)) overnight 4°C. A negative IgG (Beyotime, A7028) was also used in immunoprecipitation to exclude artifacts of non-specific and random binding. The eluted ChIP sample and the input DNA were subjected to qPCR assays to assess the interaction level of the indicated protein at each examined position.

Nuclear run-on (NRO)

NRO was conducted as previously described (10,11,38) and used to measure the transcription activities of the *MT* genes upon MRE circRNA overexpression. In short, after subcellular fractionation, nascent transcripts in nuclei were labeled with bromouridine triphosphate (BrUTP, Sigma, B7166) for 5 min in NRO Buffer (50 mM Tris–HCl pH 7.5, 5 mM $MgCl_2$, 150 mM KCl, 0.1% (w/v) srkosyl, 10 mM dithiothreitol and 80 units/ml RNase inhibitor (Beyotime, R0102)), isolated by anti-BrUTP (Abcam, ab1893) following the standard immunoprecipitation procedure and subjected to RT-qPCR assays. Purity of nascent RNAs was confirmed by checking the relative pre-mRNA enrichment of *MtnA* and *MtnB* in NRO samples over that in whole-cell RNA extracts.

DNA–RNA hybrid immunoprecipitation followed by cDNA conversion (DRIPc)

DRIPc was conducted as previously described (33,39,40), with some modifications, and used to investigate the potential of R-loop formation by MRE circRNAs. Cells were incubated with 1.6 ml of TE buffer (10 mM Tris pH 8 and 1 mM EDTA) containing 50 μl of 20% (w/v) SDS and 0.1 μg of proteinase K (Beyotime, ST532) at 37°C overnight. The solution was treated with 1.6 ml of phenol/chloroform/isoamyl alcohol (25:24:1) and centrifuged at 1500 × g for 5 min to collect the supernatant. A 1/10 volume of 3M NaOAc (pH 5.2) and 2.5 volume of 100% (v/v) alcohol was added into the supernatant for DNA precipitation. After being washed with 80% (v/v) alcohol for 3 times, the DNA was completely air-dried for 10 min at room temperature and dissolved into 125 μl of TE buffer. Subsequently, the DNA solution was used for sonication with an ultrasonic cell disruptor (Scientz-IID Sonicator) to obtain genomic DNA fragments between 100–300 bp. Sonicated DNA was extracted using phenol/chloroform/isoamyl alcohol and dissolved into DRIP buffer (50 mM HEPES/KOH pH 7.5, 140 mM NaCl, 5 mM EDTA, 0.1% (v/v) Triton X-100 and 1 mM PMSF). Using Protein A + G Agarose beads (Beyotime, P2055-50), the solution was precleared and immunoprecipitated with 5 μg of S9.6 antibody (Kerafast, ENH001) at 4°C for 16 h. A negative IgG (Beyotime, A7028) was also used in immunoprecipitation to exclude artifacts of non-specific and random binding. After being washed with DRIP buffer for 5 times, beads were incubated with DRIP elution buffer (50 mM Tris–HCl pH 8.0, 10 mM EDTA and 1% (w/v) SDS) at 55°C for 20 min to elute R-loops. The R-loop solution was treated with DNase I to digest the DNA in R-loops and incubated with a 1/10 volume of 3 M NaOAc (pH 5.2) and 2.5 volume of 100% (v/v) alcohol to precipitate RNA for 1 h at −20°C. Finally, the RNA sample was subjected to RT-qPCR assays for detection of MRE circRNAs in R-loops.

Cross-linking immunoprecipitation (CLIP)

CLIP experiments were performed as previously described (27,41,42) and used to examine the binding of gawky or Hlc to MRE circRNAs. After being washed with 1 × PBS buffer for 3 times, cells were cross-linked by UV light on ice for 2 min (254nm, 400 mJ/cm^2) and lysed in ice-cold RIPA buffer containing 80 units/ml RNase inhibitor (Beyotime, R0102) and 1 × Protease Inhibitor Cocktail (Beyotime, P1045) for 30 min. After 50 rounds of vigorous pipetting, cell lysates in the supernatant were obtained by centrifugation at 13 000 × g for 10 min at 4°C. A portion of the supernatant was preserved as the input sample for western blotting and RNA extraction, and the rest was incubated with the indicated antibody fol-

lowing the standard immunoprecipitation procedure. Afterwards, the immunoprecipitated sample was resuspended into 100 μl of RIPA buffer, 15 μl of which was used for western blotting analyses and 85 μl of which was added into RNAiso Plus (Takara, 9109) for RNA extraction followed by high-throughput sequencing or RT-qPCR assays. These antibodies were utilized in CLIP assays: anti-gawky (previously described in (11)), anti-Hlc (previously described in (10)) and anti-FLAG (Beyotime, AF519). A negative IgG (Beyotime, A7028) was also included in each immunoprecipitation reaction as a control to eliminate artifacts of random interactions.

High-throughput sequencing and bioinformatics analyses

For RNA-seq, RNAs were purified from regular S2 and MRE circRNA stable cells, and RNA quality was verified using the Agilent Bioanalyzer 5400 system. Libraries were generated with 1 μg of RNA using NEBNext® Ultra™ II RNA Library Prep Kit for Illumina® (New England Biolabs, E7775) and were subject to 150 bp paired-end sequencing using the Illumina NovaSeq 6000 system. For circRNA-seq, RNAs were purified from whole-cell extracts, nuclei and cytoplasm of regular S2 cells, and RNA quality was checked using the Agilent Bioanalyzer 5400 system. Afterwards, ribosomal RNAs were removed using TruSeq® Stranded Total RNA Library Prep Gold (Illumina, 20 020 599), and linear transcripts were digested with 3 units of RNase R (Epicentre, RNR07250) per μg of RNA. Libraries were generated using NEBNext® Ultra™ Directional RNA Library Prep Kit for Illumina® (New England Biolabs, E7420), and 150-bp paired-end sequencing was then performed through the Illumina NovaSeq 6000 system. For CLIP-seq, a combined RNA sample from three independent CLIP replicates was measured using the Agilent 2100 Bioanalyzer system and the SimpliNano™ spectrophotometer (GE Healthcare) for RNA quality controls. Subsequent library construction was performed using NEBNext® Ultra™ RNA Library Prep Kit for Illumina® (New England Biolabs, E7530). Libraries were sequenced on the Illumina Novaseq 6000 system with a paired-end read length of 150 bp.

The raw sequencing data were trimmed to remove adapter sequence contamination and low-quality reads using Trimmomatic (version 0.39) with the parameter 'SLIDINGWINDOW:5:20 LEADING:3 TRAILING:3 MINLEN:36 HEADCROP:10' (43) and examined by FastQC (version 0.11.9; http://www.bioinformatics.babraham.ac.uk/projects/fastqc/), a software providing quality control checks. For RNA-seq analyses, the remaining high-quality reads from the raw data were mapped to the reference genome (*Drosophila* melanogaster genome (BDGP6)) from Ensembl (https://www.ensembl.org) using STAR (version 2.7.10b) to generate bam files with the '–outSAMtype BAM SortedByCoordinate' parameter (44). According to the genome annotation (BDGP6.32, version 104), each sample was assessed using featureCounts (version 2.0.2) to obtain an overall gene expression matrix (45). Differential gene expression (DGE) analyses were conducted using the DESeq2 package (version 1.36.0) in the R project (46). BigWig files generated from deepTools (version 2.5.7) were used to provide Integrated Genomics Viewer (IGV) snapshots (47,48). Gene ontology (GO) analysis was performed using clusterProfiler (version 4.0.5) (49) and org.Dm.eg.db (version 3.12.0; https://www.bioconductor.org/packages/devel/data/annotation/html/org.Dm.eg.db.html) in the R project. For circRNA-seq analyses, the high-quality reads filtered from the raw data were mapped to the reference genome (*Drosophila* melanogaster genome (BDGP6)) using STAR (version 2.7.10b) with the parameter '–chimOutType Junctions SeparateSAMold' (44). The CIRCexplorer software (version 2.3.8) was then utilized to predict the BSJs of circRNAs (50). For CLIP-seq analyses, the circRIP software was used to identify circRNAs from CLIP samples (51). The BSJ reads were normalized to the exon-spanning read counts which include the exon-exon junction (EEJ) and BSJ reads. The enrichment threshold for defining gawky-interacting circRNAs is Log2 αFLAG/IgG ratio > 2.5, FLAG CLIP reads ≥ 4 and $P < 0.05$. The purpose of IGV snapshots used in the CLIP data is to show the distribution and density of the junction reads mapped to the head-to-tail joining. To generate these graphs, we applied the previously-described pseudo-reference-based pipeline (51), which needs initial establishment of pseudo-BSJ references before alignment. In brief, the sequences spanning across the circRNA BSJs (–150 to 150 bp from the BSJ) were first used for reference construction. The high-quality CLIP-seq reads were then aligned to the aforementioned pseudo-reference using Bowtie2 with the '–end-to-end' parameter (52), and the data were converted to bam files via SAMtools (version 1.3.1) (53). Finally, BigWig files were generated from the filtered bam files via deepTools (version 2.5.7) and used to provide the indicated snapshots (47,48). To ensure the validity and accuracy of the junction reads shown in IGV snapshots, they must cover at least 10 nt on each side of the head-to-tail joining. To evaluate the occurrences of the MRE motif among the sequences of 19 gawky-interacting circRNAs, the FIRE software was used in the non-discovery mode with the '–doskipdiscovery = 1 –motiffile_dna = MRE_FILE' parameter (54,55). The BSJ counts of gawky-interacting circRNAs from the FLAG CLIP sample were used as expression files with the '–expfiles' parameter, and the sequences of these circRNAs were used as input files with the '–fastafile_dna' parameter (54,55). Randomly shuffled circRNA sequences with same dinucleotide frequencies were used as the scrambled sequence control. Note that no MREs exist across BSJs of MRE circRNAs. For analyses of host mRNAs, the overall interaction was examined using featureCounts (45) followed by differential analyses using edgeR (version 3.32.1) with the 'dispersion = 0.1' parameter (56). To examine the αFLAG/IgG ratio of the reads aligned to the circularizing exons of gawky-interacting circRNAs and other exons that are not present in the circRNAs, these reads were normalized to the total read counts from their host mRNAs before calculation. For data visualization, circos plots were generated using TBtools (version 2.019) (57). Scatter plots (including bubble plots and volcano plots), box plots and cumulative fraction curves were generated by the ggplot2 package (version 3.3.5; https://cran.r-project.org/web/packages/ggplot2/). Heatmaps were generated by the pheatmap package (version 1.0.12; https://cran.r-project.org/web/packages/pheatmap/). VENN diagrams were generated through the SRplot platform (58).

Statistical analyses

Unless otherwise indicated, statistical significances for comparisons of means were tested by Student's *t*-test (**$P < 0.01$; *$P < 0.05$) and are shown in figure legends.

Results

Identification of a class of gawky-interacting circRNAs

Hypothesizing that certain circRNAs may serve as upstream regulators in the ChRBP gawky-mediated transcription activation, we sought to characterize gawky-interacting circRNAs in the presence of metal stress. To this end, we took advantage of our previously described FLAG-tagged gawky (FLAG-gawky) stable cell line (10,11) and performed CLIP-seq using copper-stressed cells with anti-FLAG (Figure 1A). The followed bioinformatics analyses showed that 19 circRNAs (defined here as gawky-interacting circRNAs) were highly associated with copper-activated gawky (Log2 αFLAG/IgG ratio > 2.5, FLAG CLIP reads ≥ 4 and $P < 0.05$) among all 334 circRNAs identified in the CLIP sample (Figure 1B, C). The CLIP-seq reads aligned to the circularizing exons of the interacting circRNAs were more enriched than those mapped to other exons that are not present in the circRNAs, confirming the validity of our CLIP-seq data (Supplementary Figure S1A). MREs were originally considered as important regulatory DNA elements located in the promoters and/or gene bodies of thousands of metal-responsive genes (59,60). Unexpectedly, using the FIRE software (54,55), we found that the MRE motif was enriched in the RNA sequences of gawky-interacting circRNAs over the scrambled sequence control (Figure 1D). Notably, 10 out of 19 (52.6%) contained perfectly matched MREs (Supplementary Figure S1B) and were referred to MRE circRNAs herein. Distinct from gawky, the DEAD-box RNA helicase Hlc has been identified as an essential transcription regulator which can specifically maintain the basal, but not stress-induced, transcription of stress-responsive genes (10). We thus asked whether Hlc binds to MRE circRNAs and performed CLIP-seq using unstressed FLAG-tagged Hlc (FLAG-Hlc) stable cells (10). In contrast to FLAG-gawky, FLAG-Hlc exhibited a very limited binding capacity towards MRE circRNAs, although *circCG32369(2)* and *circzfh2(4,5,6)* appear to mildly interact with Hlc (Figure 1E, F; Supplementary Figure S1C,D). The sequences of MRE circRNAs overlap with those of their linear counterparts, but no evident enrichment of the host mRNAs was observed in the FLAG-gawky CLIP sample (Figure 1E,F; Supplementary Figure S1C-E). CLIP-qPCR of all MRE circRNAs using antibodies against the endogenous gawky and Hlc verified the aforementioned CLIP-seq data (Figure 1G, rows 1–4). Moreover, we found that MRE circRNAs did not bind to unstressed gawky or stressed Hlc (Figure 1G, rows 5–8; Supplementary Figure S1F). These data collectively suggest the specificity of the MRE circRNA–gawky interaction.

Due to lacking of 5′ and 3′ ends, circRNAs are stable molecules (34–36). Indeed, the transcription inhibition assay confirmed that MRE circRNAs were more resistant to degradation compared to their host mRNAs (Figure 1H; Supplementary Figure S2). Besides, using the standard curve based method, the total copy number of MRE circRNAs was estimated to be between 600–1000 per cell. To investigate the nuclear-cytoplasmic distributions of MRE circRNAs, we next performed circRNA-seq experiments using RNA samples isolated from nuclei, cytoplasm and whole cells, and found that MRE circRNAs existed in both the nuclear and cytoplasmic fraction (Figure 1I). RNA-FISH of *circCG32369(2)* and *circpxb(3,4)* further confirmed the circRNA-seq data at the single-cell level (Figure 1J, K; Supplementary Figure S3A, B). The specificity of each circRNA FISH probe was verified by RNAi experiments (Supplementary Figure S3C,D). These observations suggest that MRE circRNAs are a class of nucleocytoplasmic shuttling RNA molecules. In support of this, the Nuc/Cyto ratios of all MRE circRNAs were revealed to be robustly declined in response to copper treatment (Figure 1L–N; Supplementary Figure S3E, F). No obvious changes in their total expression levels were detected (Figure 1L). The nuclear-cytoplasmic distributions of two reference circRNAs, *circdati(2)* and *circlaccase2(2)*, were not affected (Figure 1L), which served as negative controls. Of note, copper treatment had no impact on the Nuc/Cyto ratios of the host mRMAs of MRE circRNAs (Supplementary Figure S3G), further indicating the specificity of the nuclear export pattern of MRE circRNAs in response to stressed conditions.

Taken together, our results demonstrate that MRE circRNAs are a class of stress-responsive circRNAs and specifically interact with gawky under metal-stressed conditions.

MRE circRNAs attenuate stress-induced transcription

In order to explore the function of MRE circRNAs in regulating stress-responsive genes, we developed two MRE circRNA overexpression reporters by individually inserting the circularizing sequences of *circCG32369(2)* and *circMCPH1(2,3,4,5)* into the Hy_pAct5C laccase2 MCS exon vector (modified from (27,37)), in which the complementary intronic repeats can efficiently promote the back-splicing reaction of MRE circRNAs (Figure 2A). *CircCG32369(2)* and *circMCPH1(2,3,4,5)* were selected as representatives based on their variable lengths and exon numbers (Supplementary Figure S1B). The MRE circRNA stable cell lines were then constructed using these reporters with S2 cells (Figure 2A), and were ascertained to overexpress *circCG32369(2)* or *circMCPH1(2,3,4,5)* by the subsequent RT-qPCR experiment (Figure 2B).

Intriguingly, in comparison with the regular S2 cell control, the mRNA levels of the *MT* genes (a type of well-characterized metal stress-inducible genes) were robustly down-regulated in cells stably overexpressing MRE circRNAs during copper stress (Figure 2C). RNA-FISH of *MtnA* and *MtnB* mRNAs showed a similar phenotype at the single-cell level (Figure 2D, E). Differently, *MT* expression stayed largely unchanged upon overexpression of control circRNAs containing no MRE, excluding the possibility that other parts of the overexpression reporters or the method by which the stable cell lines were made caused the phenotype (Figure 2F,G). We also constructed a reporter which can exclusively produce the linear output of *CG32369* or *MCPH1*, whose sequence is identical to that of *circCG32369(2)* or *circMCPH1(2,3,4,5)*. As observed, the stress-induced expression of *MT* was not altered in these linear RNA stable cell lines (Figure 2F, G). Therefore, it is not likely that the linear version of MRE circRNAs might contribute to the down-regulation. Note that many circRNAs were found to affect the life cycle of mRNA post-transcriptionally (61–63). For example, a circRNA generated from the homeodomain-interacting protein kinase 3 (*HIPK3*) gene can enhance the stability of *AQP3* mRMA by repressing *miR-124* activity as a sponge molecule (61). However, in our case, neither the half-lives (Supplementary Figure S4) nor nuclear-cytoplasmic distributions (Supplementary Figure S5)

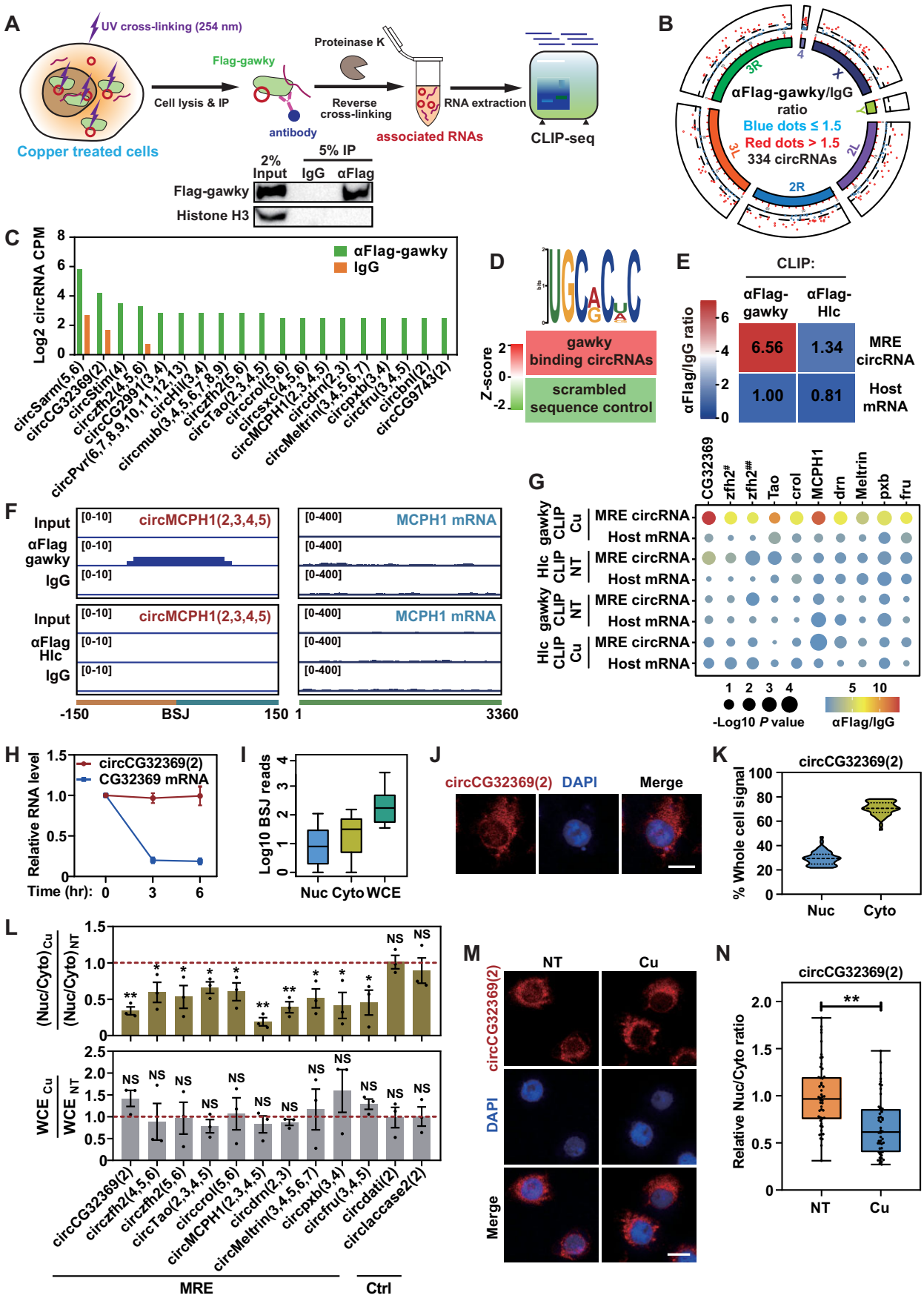

Figure 1. Identification of MRE circRNAs. (**A**) Schematic diagram of the CLIP-seq workflow for identification of gawky-interacting RNAs. Representative western blot of FLAG-tagged gawky (FLAG-gawky) for validation of the CLIP efficiency is also shown at the bottom. Histone H3 was used as a negative

of *MT* mRMAs were significantly influenced upon MRE circRNA overexpression. These data thus exclude that MRE circRNAs may regulate *MT* expression by modulating their stability or nuclear export.

Informed by the aforementioned observations and the function of gawky, we next investigated whether *circCG32369(2)* and *circMCPH1(2,3,4,5)* modulate the transcription activities of *MT* by NRO assays, in which the newly-generated *MT* transcripts were labeled with BrUTP, isolated with anti-BrUTP and examined by RT-qPCR (Figure 2H). The reference genes *18S*, *Act42A* and *αTub84B* were also examined to minimize technological artifacts of three independent NRO experiments and rule out the possibility of a global defect in Pol II transcription (Figure 2I). The measured mRNA precursors (pre-mRNAs) were substantially enriched in the NRO samples with high reproducibility (Supplementary Figure S6), eliminating the possibility of steady-state RNA contamination. Importantly, MRE circRNA overexpression led to a significant reduction in the nascent transcript abundance of all *MT* mRMAs examined (Figure 2I), supporting that MRE circRNAs, at least for *circCG32369(2)* and *circMCPH1(2,3,4,5)*, can function as potent transcription inhibitors in response to copper stress.

We also individually knocked down MRE circRNAs with the siRNAs targeting the BSJ site (Supplementary Figure S7A). RT-qPCR confirmed that MRE circRNAs, rather than their linear counterparts, were efficiently depleted (Supplementary Figure S7B). Unexpectedly, the levels of *MT* mRMAs were mostly unaffected or merely slightly increased in each knockdown sample (Supplementary Figure S7C), suggesting that loss-of-function of a single MRE circRNA is not sufficient to provoke *MT* transcription. This could be due to the functional redundancy and pleiotropic effects of these MRE circRNAs in the regulation of stress-induced transcription.

The functional activity of MRE circRNAs requires the presence of gawky

Since promoters are essential sequences that provide various regulatory signaling hubs in coordinating the transcription programmes of stress-responsive genes (64,65), we next asked whether the fate of undergoing MRE circRNA-mediated transcription repression is encrypted in the promoter regions. To test this, we made use of the previously described three-exon mini-*dati* gene vectors which are under the control of the *MT* promoters (10,11,35,66) and introduced them into MRE circRNA stable cells. Note that the mini-*dati* gene can produce not only linear RNAs (linear splicing of exon 1–3) but also circRNAs (back-splicing of exon 2) (Supplementary Figure S8A). The levels of linear and circular *dati* RNA were then evaluated by RT-qPCR after cells had been stressed with copper sulfate for 30 min. Compared to the regular S2 cell control, the expression levels of the mini-*dati* gene in the two MRE circRNA stable cell lines were significantly repressed (Supplementary Figure S8B), which resembled the phenotype from the endogenous *MT* (Figure 2C). By contrast, the *dati* promoter-driven expression was not altered upon MRE circRNA overexpression (Supplementary Figure S8B), which served as a negative control. We also noticed that the levels of linear and circular *dati* RNA were declined to a similar extent to each other (Supplementary Figure S8B), suggesting that MRE circRNA-mediated regulation is independent of different splicing patterns. Collectively, these data clearly demonstrate that the accurate role of MRE circRNAs in transcription relies on the promoter contexts. Recalling that (i) MRE circRNAs specifically interact with gawky (Figure 1A–G; Supplementary Figure S1), and (ii) gawky regulates transcription activation of metal-responsive genes through their promoters (11), we reasoned that MRE circRNAs and gawky may be functionally coupled to some extent. In the subsequent investigations, we used the model gene *MtnB* as a readout to

←

control. (**B**) Circos plot reflecting the interaction (defined as the αFLAG-gawky/IgG ratio) and genomic distribution of all 334 co-precipitated circRNAs from the FLAG-gawky CLIP sample. CircRNAs with a ratio over 1.5 are highlighted as red dots, and others are labeled as blue dots. (**C**) Bar plots showing the counts per million BSJ reads (CPM) of 19 highly enriched circRNAs from the FLAG-gawky CLIP sample. Note that the BSJ reads were normalized to the exon-spanning read counts (including both the EEJ and BSJ reads). Threshold used to define gawky-interacting circRNAs is Log2 αFLAG/IgG ratio > 2.5, FLAG CLIP reads ≥ 4 and $P < 0.05$. *P* value was calculated by binomial test. (**D**) Heatmap describing the enrichment score of the MRE motif among the sequences of gawky-interacting circRNAs, relative to the scrambled sequences (as a negative control) with same dinucleotide frequencies. The enrichment score was calculated using FIRE (54,55). (**E**) Heatmap describing the interaction levels of MRE circRNAs as well as their host mRNAs from the FLAG-gawky CLIP sample. The CLIP-seq assay with an antibody against FLAG-tagged Hlc (FLAG-Hlc) was also conducted to verify the specificity of the gawky-MRE circRNA interplay. Number inside each cell of the heatmap represents the mean of the data. (**F**) Integrative Genomics Viewer (IGV) snapshots showing the reads aligned to the head-to-tail joining of a representative MRE circRNA (*circMCPH1(2,3,4,5)*) from the FLAG-gawky and FLAG-Hlc CLIP samples (left panel). The mRNA reads spanning across the entire linear *MCPH1* transcript are also shown to exclude the possibility of non-specific binding (right panel). (**G**) CLIP-qPCR analyses of MRE circRNAs and their linear counterparts using antibodies against the endogenous gawky and Hlc. Data were generated from three independent experiments. *P* value was calculated by Student's t-test. The circular transcript of *zfh2*$^{\#}$ represents *circzfh2(4,5,6)*, and that of *zfh2*$^{\#\#}$ represents *circzfh2(5,6)*. NT: unstressed; Cu: copper-stressed. (**H**) RT-qPCR quantification of *circCG32369(2)* and *CG32369* mRNA in S2 cells that are treated with the transcription inhibitor Actinomycin D for the indicated amounts of time (0–6 h). The RNA level observed at 0 hr of Actinomycin D treatment was set to '1'. Data were generated from six independent experiments and are shown as means ± SEM. (**I**) Boxplots depicting the BSJ read counts of MRE circRNAs in the circRNA-seq data generated from nuclei (Nuc), cytoplasm (Cyto) and whole-cell extracts (WCE) of S2 cells. Each whisker extends at most 1.5 times interquartile range away from the box. (**J**, **K**) RNA FISH assays of a representative MRE circRNA (*circCG32369(2)*) with a probe against its BSJ in individual S2 cells (**J**). Representative images from three independent confocal imaging analyses are shown. Scale bar = 5 μm. The relative proportion of nuclear and cytoplasmic *circCG32369(2)* was then calculated from 50 cells and is shown in the violin plots (**K**). Lines inside each violin plot represent the first quartile, median and third quartile of the data. (**L**) RT-qPCR analyses comparing the relative Nuc/Cyto ratios of MRE circRNAs in unstressed and copper-stressed S2 cells (higher panel). The expression levels of MRE circRNAs were also measured using whole-cell extracts from the same samples (lower panel). The unstressed control was set to '1'. Data were generated from three independent experiments and are shown as means ± SEM. Each replicate is represented as a black dot. *P* value was calculated by Student's *t*-test (** $P < 0.01$; * $P < 0.05$). NT: unstressed; Cu: copper-stressed. (M, N) RNA FISH assays of *circCG32369(2)* using S2 cells treated with or without copper sulfate (**M**). Representative images from three independent confocal imaging analyses are shown. Scale bar = 5 μm. The nuclear and cytoplasmic FISH signals of *circCG32369(2)* were quantified from 50 cells. The relative Nuc/Cyto ratios were then calculated and are represented as black dots (**N**). The mean of the unstressed control was set to '1'. The minimum, median and maximum of the data are also shown in each box plot. *P* value was calculated by Student's *t*-test (** $P < 0.01$; * $P < 0.05$). NT: unstressed; Cu: copper-stressed.

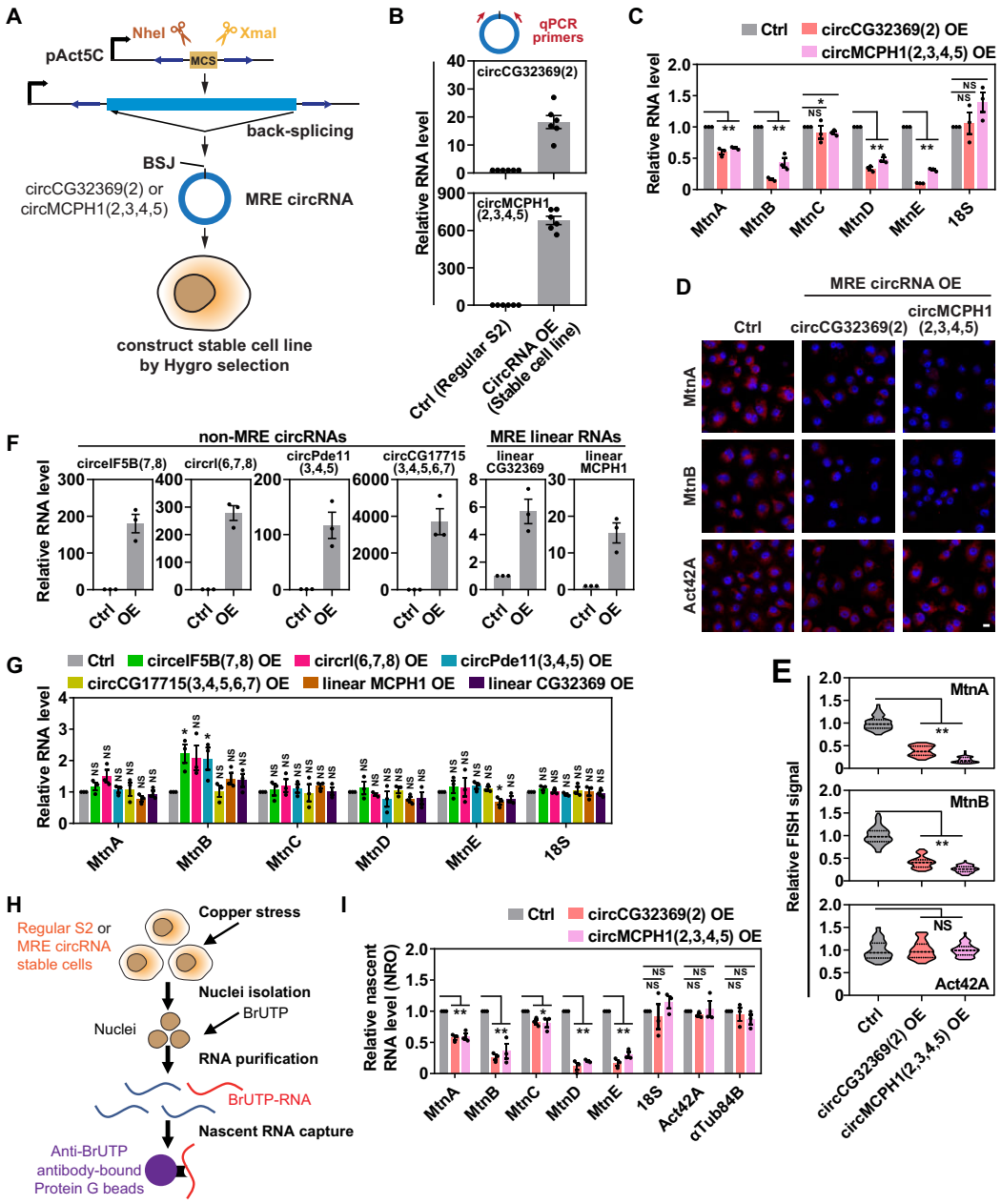

Figure 2. MRE circRNAs are potent inhibitors of stress-induced transcription. (**A**) Schematic overview of the strategy for constructing MRE circRNA stable cell lines. Briefly, the DNA sequences for producing *circCG32369(2)* and *circMCPH1(2,3,4,5)* were individually inserted between the Nhe I and Xma I sites of the Hy_pAct5C laccase2 MCS exon vector, a plasmid modified from (27,37). The generated overexpression vectors, harboring a hygromycin resistance (HygroR) cassette, were then used for stable cell selection with the assistance of hygromycin B for at least 3 weeks. (**B**) RT-qPCR quantification of *circCG32369(2)* and *circMCPH1(2,3,4,5)* verifying their overexpression efficiencies in each stable cell line. The regular S2 cell control was set to '1'. Data were generated from six independent experiments and are shown as means ± SEM. Each replicate is represented as a black dot. (**C**) RT-qPCR quantification of *MT* mRNAs in copper-treated regular S2 and MRE circRNA stable cells. The regular S2 cell control was set to '1'. Data were generated from three independent experiments and are shown as means ± SEM. Each replicate is represented as a black dot. *P* value was calculated by Student's *t*-test (** $P < 0.01$; * $P < 0.05$). (D, E) RNA FISH assays of *MtnA* and *MtnB* mRNAs in copper-treated regular S2 and MRE circRNA stable cells (**D**). Representative images from three independent confocal imaging analyses are shown. Scale bar = 5 μm. The relative expression levels of *MtnA* and *MtnB* mRNAs were then quantified from 50 cells and are shown in the violin plots (**E**). Lines inside each violin plot represent the first quartile, median and third quartile of the data. *P* value was calculated by Student's *t*-test (** $P < 0.01$; * $P < 0.05$). (**F**) RT-qPCR quantification of four control circRNAs (*circeIF5B(7,8)*, *circrl(6,7,8)*, *circPde11(3,4,5)* and *circCG17715(3,4,5,6,7)*) and two MRE linear RNAs (linear *CG32369* and *MCPH1*) verifying their overexpression efficiencies in the indicated stable cell lines. The regular S2 cell control was set to '1'. Data were generated from three independent experiments and are shown as means ± SEM. Each replicate is represented as a black dot. (**G**) RT-qPCR quantification of *MT* mRNAs in copper-treated regular S2 and stable cells described in (F). The regular S2 cell control was set to '1'. Data were generated from three independent experiments and are shown as means ± SEM. Each replicate is represented as a black dot. *P* value was calculated by Student's *t*-test (** $P < 0.01$; * $P < 0.05$). (**H**) Schematic representation of the NRO assay, adapted from (38), CC BY 4.0 (https://creativecommons.org/licenses/by/4.0/). (**I**) NRO-qPCR analyses of the newly-synthesized (BrUTP-labeled) *MT* mRNAs (i.e. evaluation of the transcription activities of the *MT* genes) in copper-treated regular S2 and MRE circRNA stable cells. The reference genes *18S*, *Act42A* and *αTub84B* were used as negative controls to assess the technological artifact in each replicate. Data were generated from three independent experiments and are shown as means ± SEM. Each replicate is represented as a black dot. *P* value was calculated by Student's *t*-test (** $P < 0.01$; * $P < 0.05$).

unveil the exact molecular details of MRE circRNAs in transcription regulation.

We first explored the functional relevance between gawky and MRE circRNAs. To avoid the potential off-target effects of the RNAi technique, we applied two independent dsRNAs to individually knock down the expression of gawky in copper-stressed regular S2 and MRE circRNA stable cells (Figure 3A). Western blotting experiments confirmed the high knockdown efficiency of the dsRNA used in each sample (Figure 3B, C). Next, *MtnB* expression was measured by RT-qPCR assays with primer sets analyzing 5′ end, middle or 3′ end of *MtnB* mRNA (Figure 3D). In line with Figure 2, overexpression of MRE circRNAs caused a robust reduction in the level of *MtnB* mRNA in β-gal dsRNA (a control dsRNA) treated cells (Figure 3E, higher panel). By contrast, MRE circRNAs failed to repress *MtnB* transcription in gawky-depleted cells (Figure 3E, middle and lower panel). The phenotype remained largely unchanged irrespective of which primer set was applied (Figure 3E). Because *MtnB* is a Pol II transcribed gene, we also monitored the overall occupancy of Pol II at the *MtnB* locus by Pol II ChIP assays using the same primer sets described in Figure 3D. Likewise, overexpression of MRE circRNAs no longer affected the binding of Pol II to *MtnB* in the absence of gawky (Figure 3F). Taken together, these results suggest that the presence of gawky is a prerequisite for the inhibitory effects of MRE circRNAs on stress-induced transcription.

It is now known that Hlc is bypassed from stress-induced transcription, but possesses a readily-detectable binding capacity towards the promoter-proximal regions of stress-responsive genes under normal conditions (10). Therefore, we sought to examine whether Hlc is involved in MRE circRNA-mediated transcription repression by Hlc knockdown experiments (Supplementary Figure S9A-C). As observed, both *circCG32369(2)* and *circMCPH1(2,3,4,5)* were still fully functional when copper-stressed cells were depleted of Hlc (Supplementary Figure S9D,E), supporting that MRE circRNAs function in an Hlc independent manner.

MRE circRNAs modulate the molecular actions of gawky

Reminiscent of the molecular mechanism by which gawky activates transcription (11), we determined whether the overall binding of gawky to the *MtnB* locus was modulated by MRE circRNAs through ChIP assays with an antibody against the endogenous gawky. A series of primer sets spanning across the TSS of *MtnB* were thereafter used to evaluate ChIP signals through qPCR experiments. In comparison with the negative IgG control, a strong interaction between gawky and the *MtnB* promoter (approximately 0–600 bp upstream of the TSS) was observed in copper-stressed regular S2 cells (Figure 4A, grey line), which was consistent with the previously reported result (11). More importantly, we found that the gawky ChIP signals were drastically reduced in cells stably overexpressing MRE circRNAs (Figure 4A, pink and purple lines), despite no significant difference in the total expression level of gawky being detected (Figure 4B, C). These data suggest that MRE circRNAs impair gawky recruitment to the active gene loci. Knowing that gawky is required for the loading of heavy metal-activated MTF-1 to stress-responsive genes (11), we also performed MTF-1 ChIP and found that the MTF-1-*MtnB* interplay was similarly destabilized in MRE circRNA stable cells during copper stress (Supplementary Figure S10A). On the contrary, MRE circRNAs had almost no effect on the binding of Hlc to the genomic *MtnB* under unstressed conditions (Supplementary Figure S10B), confirming the specificity of MRE circRNA-mediated regulation in stress-induced transcription.

The Nuc/Cyto ratio of gawky was up-regulated upon copper treatment (Figure 4D, E), and the nuclear translocation of metal-activated gawky is important for its precise regulatory activity in transcription (11). We thus addressed whether MRE circRNAs regulate the nucleocytoplasmic shuttling ability of gawky. Intriguingly, immunofluorescence staining assays showed that MRE circRNA overexpression resulted in a strong cytoplasmic accumulation of the vast majority of gawky under copper-stressed conditions (Figure 4F,G). Recalling that MRE circRNAs are stress-responsive molecules whose Nuc/Cyto ratios were decreased after copper treatment (Figure 1L–N; Supplementary Figure S3E,F), we speculated that MRE circRNAs may somehow function as a gawky carrier for the efficient nuclear export of gawky and/or preventing gawky from moving into the nucleus. Indeed, overexpression of gawky led to a significant reduction in the Nuc/Cyto ratios of most MRE circRNAs (9 out of 10) (Figure 4H–J).

Emerging studies have revealed that some circRNAs can directly regulate Pol II transcription by forming stable R-loops at the genome (30–33). However, none of endogenous MRE circRNAs were enriched by the R-loop-specific S9.6 antibody relative to the negative IgG control (Supplementary Figure S11), thereby excluding the assumption that MRE circRNAs might function at stress-responsive genes through R-loop formation.

Taken together, our data provide evidence that MRE circRNAs specifically regulate stress-induced transcription by modulating the molecular actions of gawky (i.e. releasing gawky from stress-responsive genes and enhancing its cytoplasmic accumulation).

The MRE motif is important for the accurate function of MRE circRNAs in transcription repression

Based on the fact that MRE circRNAs consist of perfectly marched MRE motifs, we assumed that MREs may contribute to the inhibitory role of MRE circRNAs in stress-induced transcription. To corroborate the model, *circCG32369(2)*, harboring two MREs in its sequence (Figure 5A; Supplementary Figure S12), was chosen to explore whether MREs function as RNA regulons. A mutant *circCG32369(2)* vector, in which the two MREs were both mutated, was generated and used for stable cell line construction (Figure 5A). We first performed gawky CLIP assays to compare the extent of the *circCG32369(2)*-gawky interaction in the wild-type and mutant *circCG32369(2)* stable cell lines. Of note, relative to the wild-type control, the *circCG32369(2)* mutant only exhibited a limited binding capacity towards gawky during copper stress (Figure 5B). The phenotype was not a result of an altered *circCG32369(2)* abundance after MRE mutation, since we observed no obvious difference in the overexpression efficiencies of the wild-type *circCG32369(2)* and its MRE mutant (Figure 5C). Therefore, these findings indicate that the *circCG32369(2)*-gawky interaction relies on MREs located in the circRNA.

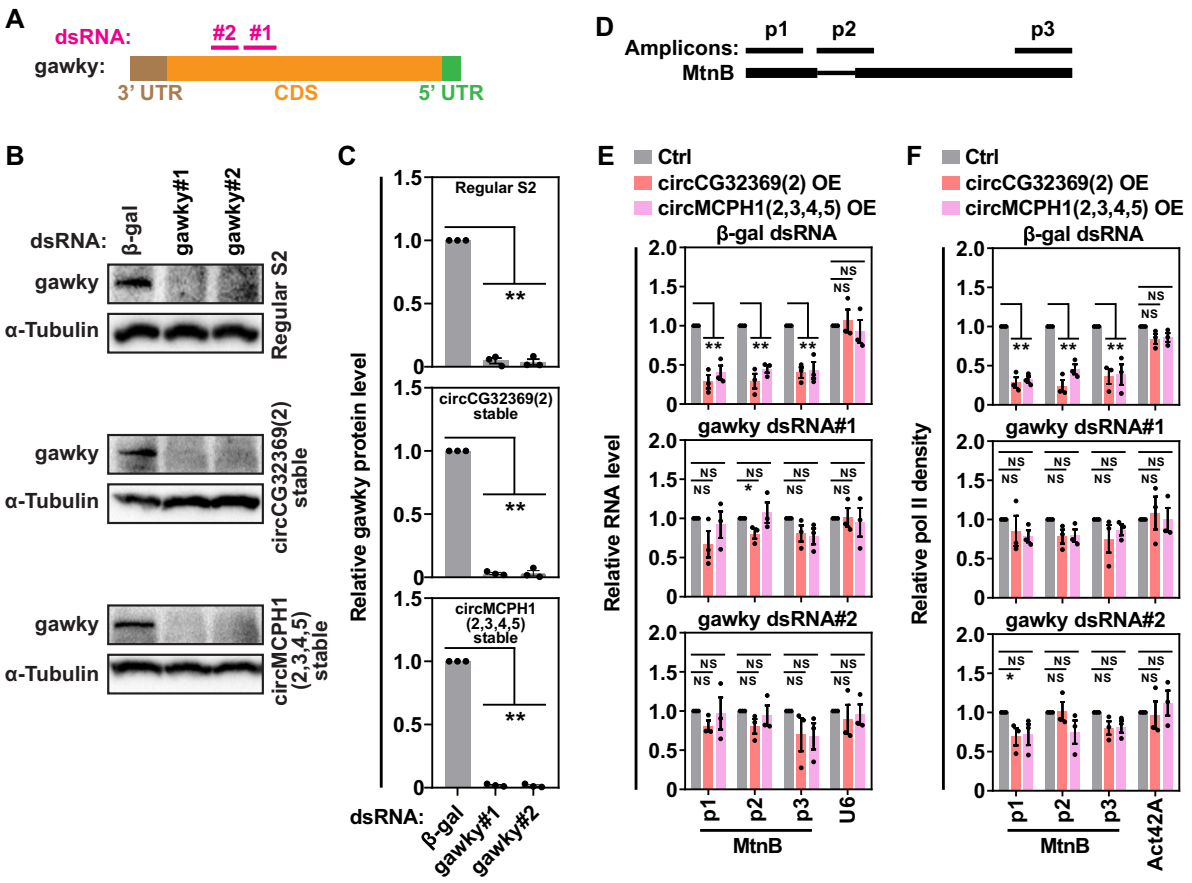

Figure 3. MRE circRNAs function in gawky-mediated transcription. (**A**) The approximate positions (marked with pink lines) of two independent dsRNAs which were used for RNAi-directed knockdown of gawky. (B, C) Representative western blots of the endogenous gawky for validation of the knockdown efficiencies of the two independent gawky dsRNAs in copper-stressed regular S2 (higher panel) and MRE circRNA stable cells (middle and lower panel) (**B**). β-gal dsRNA was used as a control dsRNA for RNAi experiments. α-Tubulin was used as a loading control for western blotting assays. The protein levels of gawky were quantified from three independent blots (**C**). Data are shown as means ± SEM, and each replicate is represented as a black dot. *P* value was calculated by Student's *t*-test (** $P < 0.01$; * $P < 0.05$). (**D**) The approximate positions of primer sets for detecting the 5′ end (p1), middle (p2) and 3′ end (p3) of the *MtnB* gene body. (**E**) Related to (A–D), RT-qPCR analyses measuring the extent of the inhibitory effect of MRE circRNA overexpression on the *MtnB* mRNA level in the control and gawky RNAi cells. The reference gene *U6* was used as a negative control. Data were generated from three independent experiments and are shown as means ± SEM. Each replicate is represented as a black dot. *P* value was calculated by Student's *t*-test (** $P < 0.01$; * $P < 0.05$). (**F**) Related to (A–D), Pol II ChIP assays examining the extent of the inhibitory effect of MRE circRNA overexpression on Pol II density at the genomic *MtnB* in the control and gawky RNAi cells. The reference gene *Act42A* was used as a negative control. Data were generated from three independent experiments and are shown as means ± SEM. Each replicate is represented as a black dot. *P* value was calculated by Student's *t*-test (** $P < 0.01$; * $P < 0.05$).

To further determine whether the interaction is required for MRE circRNA-mediated transcription regulation, we performed gawky ChIP assays to compare the recruitment of gawky to the *MtnB* locus in the wild-type and mutant *circCG32369(2)* stable cell lines. Consistent with our prior data (Figure 4A), overexpression of the wild-type *circCG32369(2)* triggered the release of gawky from the *MtnB* promoter (Figure 5D, grey line versus pink line). By contrast, gawky in cells overexpressing the MRE mutant exhibited an occupancy level similar to that in regular S2 cells (Figure 5D, grey line versus purple line). The overall protein level of gawky was unaffected in these cell lines (Figure 5E, F). We thus concluded that the inhibitory effect of *circCG32369(2)* on gawky recruitment to the genome needs the assistance of MREs. Upon examining the subcellular localization of gawky by immunofluorescence staining assays, we additionally found that the ability of *circCG32369(2)* in inducing cytoplasmic accumulation of stress-activated gawky was substantially impaired when its MREs were mutated, although overexpression of the MRE mutant mildly reduced the Nuc/Cyto ratio of gawky (Figure 5G,H). Accordingly, the inhibitory effect of *circCG32369(2)* on the copper-induced transcription of *MtnB* was diminished upon loss of MREs (Figure 5I). The MRE mutant of *circMCPH1(2,3,4,5)* yielded similar observations (Supplementary Figure S12, S13). It should be noticed that these MRE mutants still can slightly affect gawky and transcription (Figure 5; Supplementary Figure S13). This implies that MRE is necessary but not sufficient for the role of MRE circRNAs and additional RNA regulons might exist.

Taken together, our data prove that MREs located in the MRE circRNAs serve as a regulatory element for the circRNA-gawky interaction, which is indispensable for the precise regulation of gawky-mediated transcription during stressed conditions.

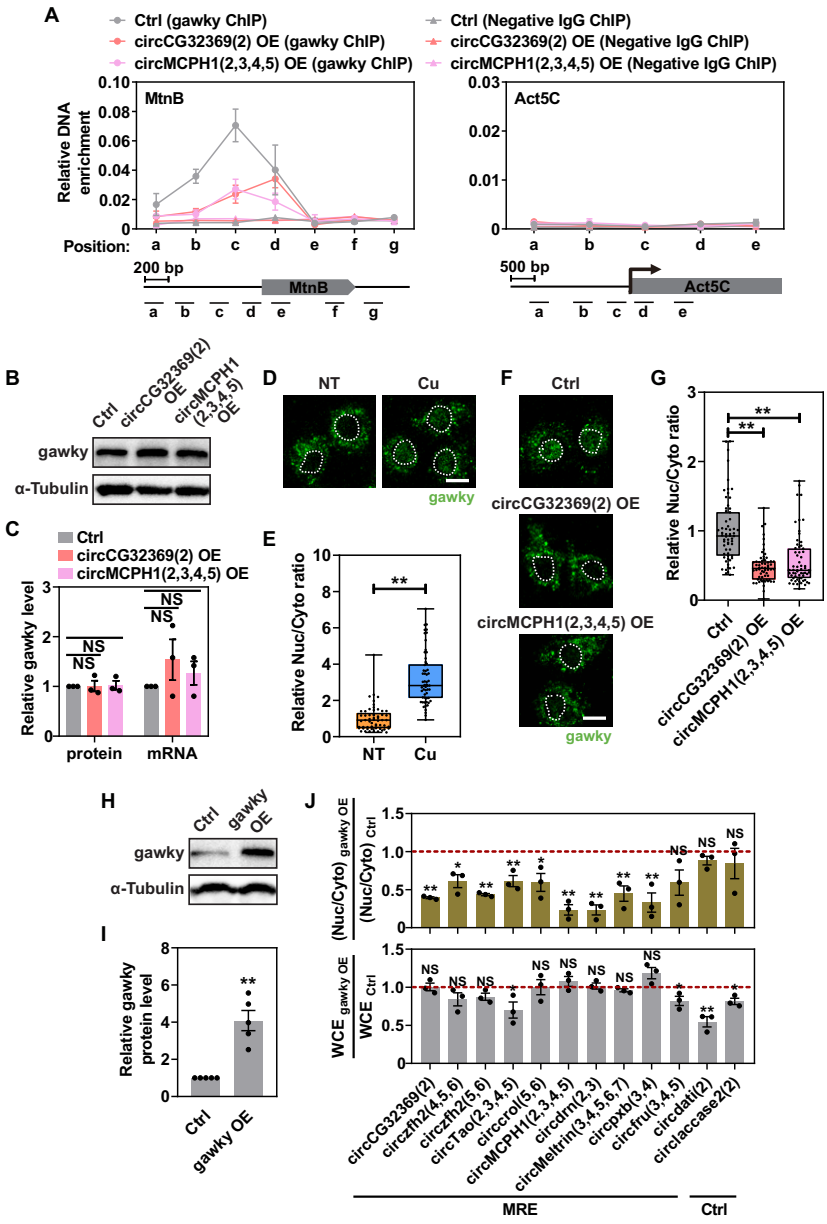

Figure 4. MRE circRNAs regulate the gawky-chromatin interaction. (**A**) Gawky ChIP assays comparing the binding of gawky to the *MtnB* locus in copper-stressed regular S2 and MRE circRNA stable cells (left panel). The house-keeping gene *Act5C* served as a control locus (right panel). The negative IgG was used to rule out artifacts of non-specific and random interactions. The interaction level at each examined position was evaluated by measuring the relative DNA enrichment of the ChIP sample over the input DNA (% input). The approximate positions of ChIP amplicons at the genomic *MtnB* and *Act5C* are shown at the bottom. Data were generated from three independent experiments and are shown as means ± SEM. (B, C) Representative western blot of gawky using whole-cell extracts from copper-stressed regular S2 and MRE circRNA stable cells (**B**). The protein levels of gawky were quantified from three independent bolts (C, left panel), and the mRNA levels of gawky were also examined by RT-qPCR using the same three independent whole-cell extracts (C, right panel). Data are shown as means ± SEM, and each replicate is represented as a black dot. *P* value was calculated by Student's t-test (** $P < 0.01$; * $P < 0.05$). (D, E) Immunofluorescence staining assays comparing the nuclear-cytoplasmic distribution of gawky in unstressed and copper-treated S2 cells (**D**). Representative images from three independent confocal imaging analyses are shown. Dashed lines indicate the border of nuclei. Scale bar = 5 μm. The nuclear and cytoplasmic fluorescence signals of gawky were quantified from 57 cells. The mean of the unstressed control was set to '1'. The relative Nuc/Cyto ratios were then calculated and are represented as black dots (**E**). The minimum, median and maximum of the data are also shown in each box plot. *P* value was calculated by Student's *t*-test (** $P < 0.01$; * $P < 0.05$). NT: unstressed; Cu: copper-stressed. (F, G) Immunofluorescence staining assays comparing the nuclear-cytoplasmic distribution of gawky in copper-treated regular S2 and MRE circRNA stable cells (**F**). Representative images from three independent confocal imaging analyses are shown. Dashed lines indicate the border of nuclei. Scale bar = 5 μm. The nuclear and cytoplasmic fluorescence signals of gawky were quantified from 62 cells. The mean of the regular S2 cell control was set to '1'. The relative Nuc/Cyto ratios were then calculated and are represented as black dots (**G**). The minimum, median and maximum of the data are also shown in each box plot. *P* value was calculated by Student's *t*-test (** $P < 0.01$; * $P < 0.05$). (H, I) Representative western blot of gawky in copper-stressed regular S2 and gawky stable cells (**H**). The protein levels of gawky were quantified from five independent bolts (**I**). α-Tubulin was used as a loading control. Data are shown as means ± SEM, and each replicate is represented as a black dot. *P* value was calculated by Student's *t*-test (** $P < 0.01$; * $P < 0.05$). (**J**) RT-qPCR quantification of the relative Nuc/Cyto ratios and expression levels of MRE circRNAs in copper-stressed regular S2 and gawky stable cells. The regular S2 cell control was set to '1'. Data were generated from three independent experiments and are shown as means ± SEM. Each replicate is represented as a black dot. *P* value was calculated by Student's *t*-test (** $P < 0.01$; * $P < 0.05$).

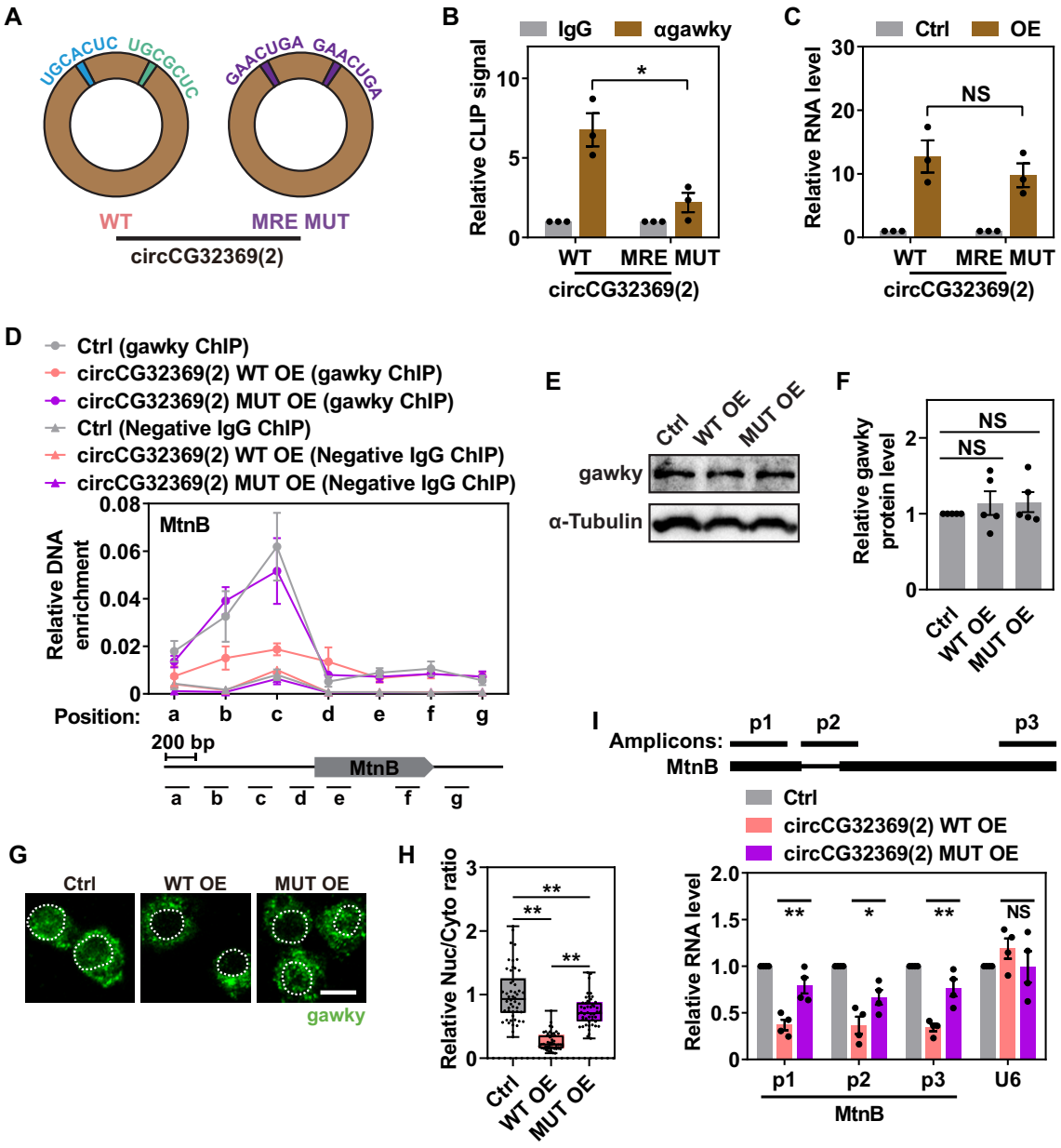

Figure 5. The MRE motif is required for MRE circRNA-mediated transcription repression. (**A**) Schematic representations of the wild-type *circCG32369(2)* (WT) and its MRE mutant (MUT) whose two MRE motifs were mutated to 'GAACUGA'. The MRE MUT stable cell line was then generated by hygromycin B selection and used for the following experiments. (**B**) CLIP assays of gawky using the WT and MRE MUT stable cell lines. RT-qPCR was then performed with RNA extracts from the CLIP samples to examine the binding of gawky to the wild-type and mutant *circCG32369(2)*. Data were generated from three independent experiments and are shown as means ± SEM. Each replicate is represented as a black dot. *P* value was calculated by Student's *t*-test (** $P < 0.01$; * $P < 0.05$). (**C**) RT-qPCR analyses comparing the overexpression efficiencies of *circCG32369(2)* in WT and MRE MUT stable cell lines. Data were generated from three independent experiments and are shown as means ± SEM. Each replicate is represented as a black dot. *P* value was calculated by Student's *t*-test (** $P < 0.01$; * $P < 0.05$). (**D**) ChIP assays comparing the binding of gawky to the *MtnB* locus in copper-treated WT and MRE MUT stable cell lines. As a positive control, the indicated interaction in regular S2 cells was also measured. The negative IgG was used to rule out artifacts of non-specific and random interactions. The interaction level at each examined position was evaluated by measuring the relative DNA enrichment of the ChIP sample over the input DNA (% input). The approximate positions of ChIP amplicons at the genomic *MtnB* are shown at the bottom. Data were generated from three independent experiments and are shown as means ± SEM. (E, F) Representative western blot of gawky using the WT and MRE MUT stable cell lines (**E**). α-Tubulin was used as a loading control. The protein levels of gawky were quantified from five independent bolts (**F**). Data are shown as means ± SEM, and each replicate is represented as a black dot. *P* value was calculated by Student's *t*-test (** $P < 0.01$; * $P < 0.05$). (G, H) Immunofluorescence staining assays comparing the nuclear-cytoplasmic distribution of gawky in copper-treated WT and MRE MUT stable cell lines (**G**). Representative images from three independent confocal imaging analyses are shown. Dashed lines indicate the border of nuclei. Scale bar = 5 μm. The nuclear and cytoplasmic fluorescence signals of gawky were quantified from 50 cells. The mean of the regular S2 cell control was set to '1'. The relative Nuc/Cyto ratios were then calculated and are represented as black dots (**H**). The minimum, median and maximum of the data are also shown in each box plot. *P* value was calculated by Student's *t*-test (** $P < 0.01$; * $P < 0.05$). (**I**) RT-qPCR analyses comparing the expression levels of *MtnB* mRNA in WT and MRE MUT stable cell lines. As a control, the *MtnB* mRNA level in regular S2 cells was also measured. The approximate positions of primer sets for detecting the 5′ end (p1), middle (p2) and 3′ end (p3) of the *MtnB* gene body are shown on top. Data were generated from four independent experiments, and each replicate is represented as a black dot. *P* value was calculated by Student's *t*-test (** $P < 0.01$; * $P < 0.05$).

MRE circRNAs play a general and potent role in regulating hundreds of copper-inducible genes during copper stress

A myriad of stress-responsive genes can be rapidly activated to combat the harmful external environment (1,2). Consistently, we found that the expression levels of a total of 1627 genes were markedly elevated upon treatment of copper sulfate (Log_2 fold change > 2 and $P < 0.05$) (Figure 6A, left panel). These genes were referred to copper-inducible genes thereafter. To substantiate the importance of MRE circRNA-mediated regulation, we next elucidated whether MRE circRNAs exert a genome-wide or limited function in transcription repression by RNA-seq assays using RNA samples isolated from copper-stressed regular S2 and *circCG32369(2)* stable cells. As observed, *circCG32369(2)* overexpression resulted in a significant and robust inhibition in 71.3% (1002 out of 1406) of differentially expressed genes (Log_2 fold change < –1 and $P < 0.05$) (Figure 6A, right panel). Notably, upon examining all 1627 copper-inducible genes, we identified a strong and global repressive effect of *circCG32369(2)* (Figure 6B), implying the selectivity of MRE circRNAs on the copper-inducible gene group. In support of this, (i) 52.4% (525 out of 1002) of the *circCG32369(2)* repressed genes belonged to copper-inducible genes (Figure 6C); (ii) copper-inducible genes were more sensitive to *circCG32369(2)*-mediated transcription regulation among these repressed genes, because the expression levels of copper-inducible genes were decreased to a much greater extent than those of non-inducible genes (Figure 6D, E); (iii) *circCG32369(2)* was more inclined to silence genes that have higher induction levels in response to copper stress, since the magnitude of the induction levels of genes was correlated with the magnitude of the down-regulation effect of *circCG32369(2)* on them (Figure 6F,G). We also analyzed the expression levels, GC content and exon numbers of the *circCG32369(2)* repressed genes in copper-stressed regular S2 cells. As shown in Figure 6H–K, the repressed genes demonstrated significantly lower expression levels and higher GC content than others. But no large difference in the exon numbers was observed between these two sets (Figure 6L, M). These findings thus indicate that genes with lower expression levels and higher GC content were more unique to the *circCG32369(2)*-involved regulatory pathway. Additionally, we found that highly-expressed genes were less sensitive to overexpression of *circCG32369(2)* (Figure 6N,O), suggesting that the observation described in Figure 6F and G was not a result of off-target effects from the very high expression levels of genes during copper stress. In line with *circCG32369(2)*, *circMCPH1(2,3,4,5)* overexpression led to similar phenotypes (Supplementary Figure S14). Taken together, our results strongly support the widespread role of MRE circRNAs in repressing stress-induced transcription and clearly reveal their selective effect on stress-inducible genes.

Informed by the finding that knockdown of a single MRE circRNA cannot promote stress-induced transcription, we reasoned that MRE circRNAs seem to have functional redundancy in the regulation (Supplementary Figure S7C). In agreement with the idea, the inhibitory effect of *circCG32369(2)* overexpression exhibited a rather significant correlation with that of *circMCPH1(2,3,4,5)* overexpression (Pearson's correlation $R = 0.4647$ and $P < 0.0001$) (Figure 6P). In particular, a total of 696 genes were found to be inhibited by both *circCG32369(2)* and *circMCPH1(2,3,4,5)* (Supplementary Figure S15A). For example, the transcription of *MFS3*, *hoe1* and *Drat* was drastically increased during copper stress, but was almost completely silent when *circCG32369(2)* and *circMCPH1(2,3,4,5)* were individually overexpressed in the cells (Figure 6Q), which was analogous to our prior data with *MT* (Figure 2). RT-qPCR of these mRNAs confirmed our RNA-seq data (Supplementary Figure S15B). Gene ontology (GO) analysis revealed that the set of the 696 co-regulated genes was enriched for the categories regarding to 'protein folding' (Supplementary Figure S15A). It is also worth mentioning that these two MRE circRNAs possess distinct selectivity on certain gene groups. For example, *circCG32369(2)* was unique in repressing genes related to 'defense response to Gram-positive bacterium', etc., while *circMCPH1(2,3,4,5)* specifically repressed genes connected with 'carbohydrate metabolic process', etc. (Supplementary Figure S15A). Collectively, these results demonstrate the combinatorial control of the transcription reprogramming of diverse genes by different MRE circRNAs.

The physiological relevance of MRE circRNAs to cellular homeostasis during copper stress

Numerous studies have demonstrated several mechanisms of copper-induced cellular toxicity, the most important one of which is based on the redox capability of copper ions in living organisms (67–71). The cuprous ion, reduced from the cupric one, is able to catalyze the generation of hydroxyl radical. As the most reactive and powerful free radical, hydroxyl radical can further drive oxidative damage and subsequent DNA strand breakages (67–70). Consistent with these prior studies, we found that an array of antioxidant defense- and DNA damage repair-related genes were significantly up-regulated in cellular defense against copper stress upon examining the RNA-seq data (Figure 7A, Cu versus NT). In addition, immunofluorescence staining analysis of the phosphorylated H2A.V (γH2A.V), a classic and straightforward method to assess the genomic integrity of individual *Drosophila* cells (72,73), showed obvious DNA damage signals in the nuclei of copper-stressed cells (Figure 7B,C).

In order to explore the potential physiological significance of MRE circRNAs, we first investigated whether MRE circRNAs affect the induction extent of oxidative stress-related genes in response to copper stress. Compared to the regular S2 cell control, all examined antioxidant defense- and DNA damage repair-related genes were substantially inhibited in the two MRE circRNA stable cell lines (Figure 7A, *circCG32369(2)* OE versus Ctrl and *circMCPH1(2,3,4,5)* OE versus Ctrl). This implicates that MRE circRNAs may have adverse effects on the cellular defense against harmful environments. Indeed, we found that overexpression of MRE circRNAs significantly aggravated copper-induced DNA damage, since the nuclear fluorescence signals of γH2A.V in MRE circRNA stable cells were much higher than those in regular S2 cells (Figure 7B, C). Moreover, we sought to compare the cellular sensitivity of regular S2 and MRE circRNA stable cells to copper stress and counted the number of living cells after copper treatment over time. As expected, overexpression of MRE circRNAs were found to significantly reduce the copper resistance of the cell (Figure 7D). Taken together, these findings confirm the physiological relevance of MRE circRNAs in promoting removal of damaged cells during copper stress.

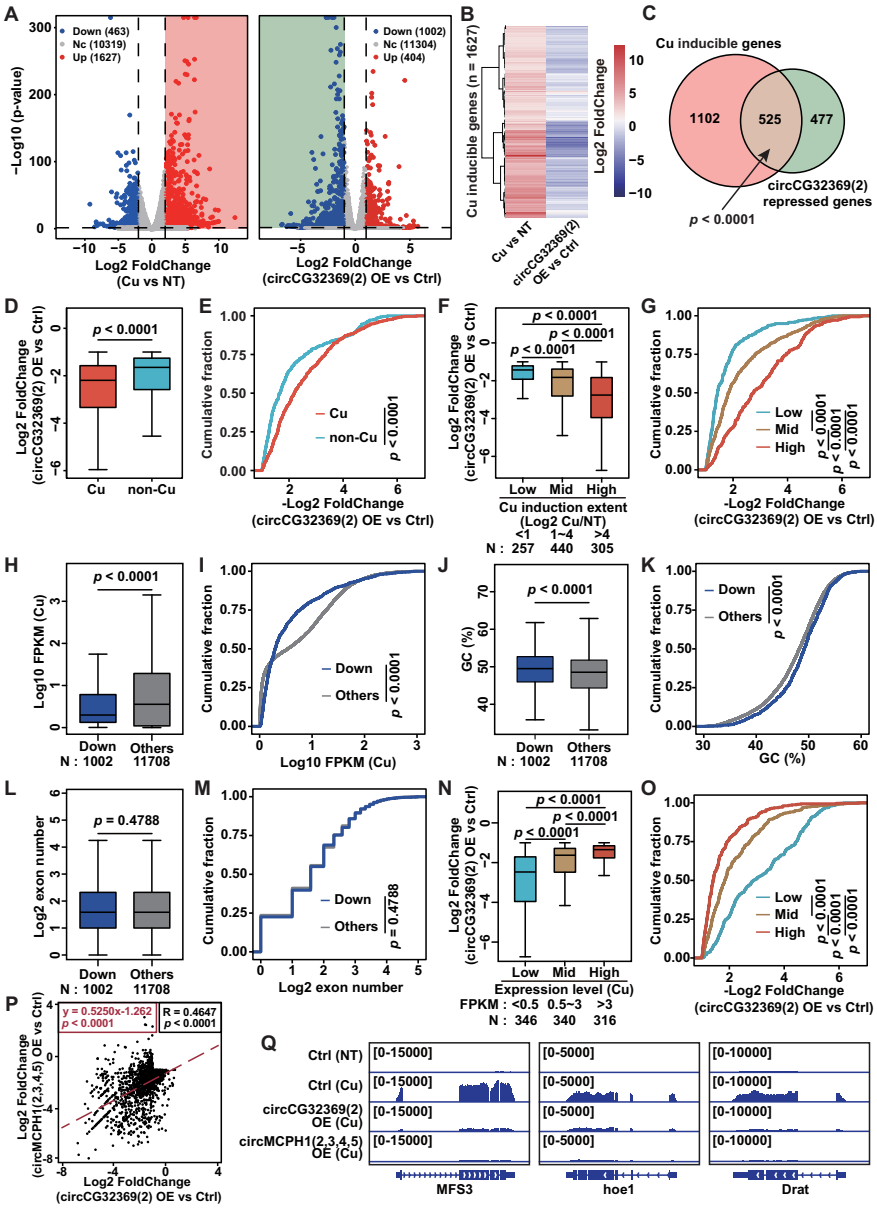

Figure 6. The repressive effects of MRE circRNAs on stress-induced transcription are pervasive for many *Drosophila* genes. (**A**) Left panel: volcano plot displaying differentially expressed genes in regular S2 cells treated with or without copper sulfate (Cu vs. NT). Threshold used to define copper-inducible genes is Log_2 fold change >2 and $P < 0.05$ ($n = 1627$). Right panel: volcano plot displaying differentially expressed genes in copper-treated *circCG32369(2)* stable and regular S2 cells (*circCG32369(2)* OE versus Ctrl). Threshold used to define *circCG32369(2)* repressed genes is Log_2 fold change < −1 and $P < 0.05$ (n = 1002). Down- and up-regulated genes in these plots are represented as blue and red dots, respectively. *P* value was calculated by Student's *t*-test. (**B**) Heatmap indicating the global repressive effect of *circCG32369(2)* on all 1627 copper-inducible genes. (**C**) Venn diagram showing the overlap between the copper-inducible gene group ($n = 1627$) and the *circCG32369(2)* repressed gene group ($n = 1002$). *P* value was calculated by Fisher's exact test. (**D**, **E**) Box plots (**D**) and cumulative fraction curves (**E**) comparing the reduction extent between copper-inducible ($n = 525$) and non-inducible ($n = 477$) genes upon *circCG32369(2)* overexpression. These genes belong to the *circCG32369(2)* repressed gene group. Each whisker, if any, extends at most 1.5 times interquartile range away from the box. *P* value was calculated by Student's *t*-test. (F, G) Box plots (**F**) and cumulative fraction curves (**G**) comparing the reduction extent between three gene sets with different degree of copper induction (Low, Mid and High; $n = 257$, 400 and 305) upon *circCG32369(2)* overexpression. These gene sets belong to the *circCG32369(2)* repressed gene group. Each whisker, if any, extends at most 1.5 times interquartile range away from the box. *P* value was calculated by Student's *t*-test. (H–M) Box plots and cumulative fraction curves comparing the expression levels (**H**, **I**), GC content (**J**, **K**) and exon numbers (**L**, **M**) of the *circCG32369(2)* repressed genes ($n = 1002$) with those of other detected genes (i.e. unchanged and up-regulated genes; $n = 11\ 708$). Each whisker, if any, extends at most 1.5 times interquartile range away from the box. *P* value was calculated by Student's *t*-test. (N, O) Box plots (**N**) and cumulative fraction curves (**O**) comparing the reduction extent between three gene sets with different expression levels (Low, Mid and High; $n = 346$, 340 and 316) upon *circCG32369(2)* overexpression. These gene sets belong to the *circCG32369(2)* repressed gene group. The expression levels of these gene sets were measured using copper-stressed regular S2 cells. Each whisker, if any, extends at most 1.5 times interquartile range away from the box. *P* value was calculated by Student's *t*-test. (**P**) Pearson correlation analysis of genes individually repressed by *circCG32369(2)* and *circMCPH1(2,3,4,5)*. The linear regression line (red) indicates the positive correlation between both gene sets (Pearson's correlation $R = 0.4647$). The fitted formula is also shown at the top-right corner. *P* values for Pearson correlation and fitted formula were calculated by Student's *t*-test and *F*-test, respectively. (**Q**) IGV snapshots of *MFS3*, *hoe1* and *Drat* expression in the indicated cell lines. The genomic locus of each gene is shown at the bottom. Ctrl (NT): unstressed regular S2 cells; Ctrl (Cu): copper-stressed regular S2 cells; *circCG32369(2)* OE (Cu): copper-stressed *circCG32369(2)* stable cells; *circMCPH1(2,3,4,5)* OE (Cu): copper-stressed *circMCPH1(2,3,4,5)* stable cells.

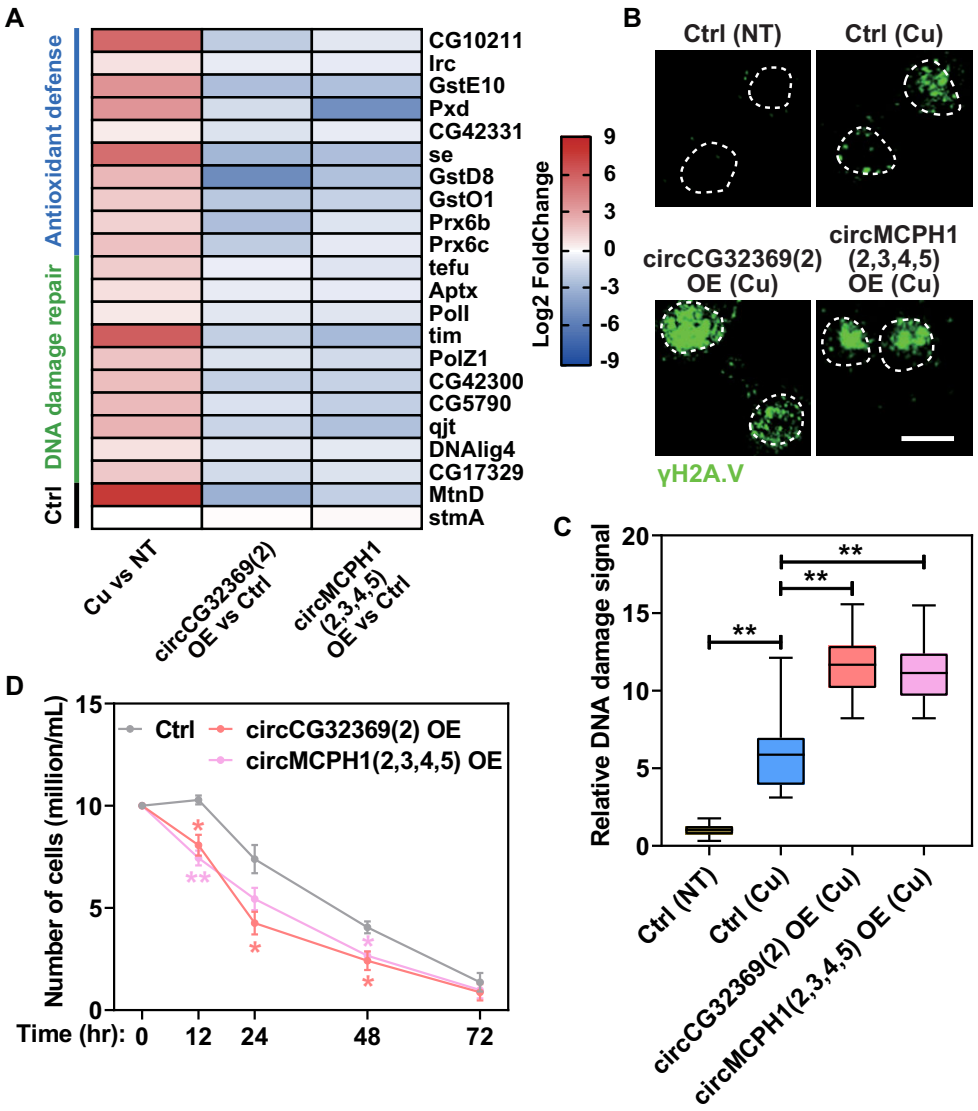

Figure 7. MRE circRNAs aggravate copper-induced DNA damage. (**A**) Heatmap reflecting the extensively repressive effects of *circCG32369(2)* and *circMCPH1(2,3,4,5)* on an array of antioxidant defense- and DNA damage repair-related genes whose expression levels were robustly increased in cellular response to copper stress. *MtnD* and *stmA* served as a positive and negative control, respectively. (B, C) Immunofluorescence staining assays measuring the DNA damage signals in the indicated cell lines (**B**). γH2A.V served as a DNA damage marker. Representative images from three independent confocal imaging analyses are shown. Dashed lines indicate the border of nuclei. Scale bar = 5 μm. The relative nuclear DNA damage signals were then quantified from 50 cells (**C**). The mean of the control sample (unstressed regular S2 cells) was set to '1'. The minimum, median and maximum of the data are also shown in each box plot. *P* value was calculated by Student's *t*-test ($^{**}P < 0.01$; $^{*}P < 0.05$). Ctrl (NT): unstressed regular S2 cells; Ctrl (Cu): copper-stressed regular S2 cells; *circCG32369(2)* OE (Cu): copper-stressed *circCG32369(2)* stable cells; *circMCPH1(2,3,4,5)* OE (Cu): copper-stressed *circMCPH1(2,3,4,5)* stable cells. (**D**) Examination of cellular resistance to copper stress. *CircCG32369(2)* and *circMCPH1(2,3,4,5)* stable cell lines were individually cultured in the medium in the presence of 1.5 mM copper sulfate over time (0–72 h), and the number of survival cells was counted. The resistance of regular S2 cells served as a negative control. *P* value was calculated by Student's *t*-test (** $P < 0.01$; * $P < 0.05$).

Discussion

The conventional view of RBPs is that they post-transcriptionally participate in gene regulation by governing the functions and/or fates of the bound RNAs (5–7). However, a subset of RBPs were recently identified as pervasive and essential components at active transcriptional loci of many eukaryotic genes (9–15). These ChRBPs have physiological roles in a broad spectrum of cellular processes and can function as non-canonical transcription regulators through diverse mechanisms, such as recruiting TFs, affecting chromatin conformations and forming membraneless compartments at the genome (9–15). It is also necessary to underline that ChRBPs are a category of multifunctional proteins, and the ChRBP-chromatin interaction is reversible and dynamic in different cellular contexts (10–15). A pertinent example in point is the ChRBP gawky which can promote RNA degradation in the cytoplasm under normal conditions (35,74), but quickly translocates into the nucleus to activate stress-induced transcription when cells sense heavy metal ions in the environment (11). These facts thus suggest that (i) the precise control of ChRBPs on chromatin is a fundamental aspect to pattern biological events, and (ii) cells should employ a sophisticated mechanism to specifically coordinate different functions of individual versatile ChRBPs. In support of the theory, this

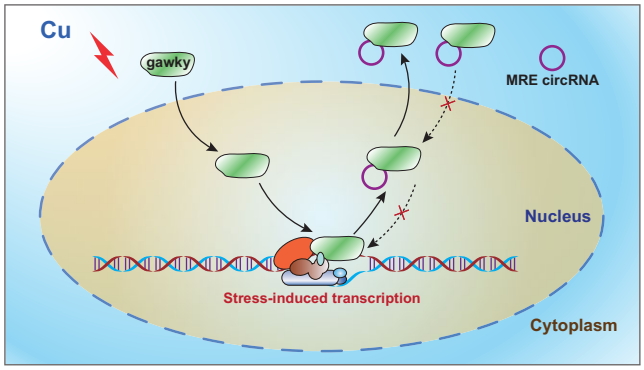

Figure 8. A working model for MRE circRNA-mediated transcription repression. MRE circRNAs inhibit stress-induced transcription by releasing the ChRBP gawky from the active genomic loci and triggering the aberrant gawky enrichment in the cytoplasmic fraction.

study proposes that MRE circRNAs negatively regulate the stress-induced transcription of hundreds of stress-responsive genes by disrupting the functional activity of stress-activated gawky on chromatin. The focused investigation on the *MtnB* gene highlights the underlying molecular details of MRE circRNA-mediated regulation: MRE circRNAs facilitate the dissociation of gawky from the active genomic regions and trigger its aberrant cytoplasmic accumulation, which further leads to a failure in the recruitment of TFs (e.g. MTF-1) and Pol II (Figure 8). The inhibitory effects of these circRNAs rely on the MRE motif, an RNA regulon required for the interaction between MRE circRNAs and gawky. Moreover, we uncovered that MRE circRNAs reduce cellular resistance to copper stress by aggravating copper-induced DNA damage, advancing our understanding of the physiological significance of ChRBP dysregulation to cell survival. In conclusion, this work, together with previous studies, demonstrates that circRNAs can serve as upstream regulators of ChRBPs and the circRNA-ChRBP interplay could provide a key bridge for the connection between transcriptional and post-transcriptional regulatory processes.

Another interesting finding in this study is the copper-induced nuclear export of MRE circRNAs (Figure 1L–N; Supplementary Figure S3E,F). Since the biogenesis of these circRNAs was not affected after copper treatment (Figure 1L), there must be additional layers of regulation to cause the re-localization. In fact, as a vital step of the life cycle of circRNAs, the regulation of circRNA transportation is essential for their proper functional activities (MRE circRNAs are the cases) and is becoming a hot topic in RNA biology. We previously reported that the evolutionarily-conserved RBPs Xpo4 (39) and DDX39A/B (66) are capable of promoting efficient nuclear export of a subgroup of circRNAs in normal/unstressed states. However, loss-of-function of these RBPs merely had limited or mild influence on the Nuc/Cyto ratios of MRE circRNAs during copper stress (data not shown). This raises a hypothesis that certain responsive circRNAs may make use of alternative export modes (or regulators) to meet extreme and stressful situations. In accordance with this conception, a previous study reported that many heat-shock linear mRNAs can be quickly exported to the cytoplasm without the assistance of adaptors that are important for the general nuclear export pathway (75). Based on these hints, we will explore what factors/pathways exclusively control circRNA export during stress in the future. Furthermore, the question of whether other stressed conditions affect the subcellular localization of MRE circRNAs (i.e. whether MRE circRNA-mediated transcription repression happens under other abnormal cellular contexts or pathological conditions) is still unknown. Therefore, to further understand the overall mechanism by which circRNAs modulate adaptive responses, additional studies are urgently required for the field of circRNA export.

The issue about how lowly-expressed circRNAs can confer effective regulation on their interacting proteins is a long-standing and unanswered question (19,20). This could be explained in part by the covalently-closed structure and excellent stability of circRNAs, which make them able to accumulate to high levels in cells (34–36). Consistently, we found that all MRE circRNAs have very long half-lives and are much more stable than their linear counterparts (Figure 1H; Supplementary Figure S2). Moreover, previous studies have suggested that functional circRNAs can act as a group to bind and modulate their target proteins (76–78). For example, multiple intron-derived circRNAs function together as a molecular decoy to seize cytoplasmic TDP43 away from other essential RNAs and RBPs, thereby decreasing TDP-43-mediated cytotoxicity in neural cells (78). In agreement with this, we revealed that the individual knockdown of endogenous MRE circRNAs was not sufficient to up-regulate stress-induced transcription (Supplementary Figure S7C), and the inhibitory effects of different MRE circRNAs showed a rather significant and high correlation between each other (Figure 6P; Supplementary Figure S15A). These data indicate the combinatorial control of stress-induced transcription reprogramming by diverse MRE circRNAs whose total copies were found to be 600–1000 per cell. In fact, using the previously-published mass spectrometry data and the histone proteomic ruler based method, a single S2 cell was inferred to have 200–240 gawky protein molecules (79–81). Therefore, the stoichiometry between MRE circRNAs and gawky can support a measurable effect. In addition, informed by the fact that certain circRNAs have multiple RBP binding sites (82), it is thus likely that dozens of gawky proteins might be accommodated by a single MRE circRNA molecule. We will examine the possibility next.

Several lines of evidence have indicated that the circRNA-RBP interplay can modulate gene output by enhancing or inhibiting the molecular functions of RBPs at the post-transcriptional stage (62,63,83). For example, the RBP IGF2BP3 can efficiently prevent *PDPN* mRNA from degradation by forming a stable ribonucleoprotein (RNP) complex with the assistance of its interactor *circITGB6* in the process of epithelial-mesenchymal transition (62); the glioblastoma-induced circRNA *circ2082* binds to Dicer and causes its aberrant nuclear retention, thereby interrupting the normal functions of Dicer in miRNA maturation (83). Nevertheless, we found that neither the stability (Supplementary Figure S4), subcellular distribution (Supplementary Figure S5) nor splicing pattern (Supplementary Figure S8) of examined mRNAs was significantly affected upon MRE circRNA overexpression. Therefore, our findings somehow rule out the assumption that MRE circRNAs might also function post-transcriptionally, at least for the control of *MT* expression. Moreover, in most cases, the linear counterparts of these regulatory circRNAs have no influence on RBPs (62,77,83,84), even though they come from the same pre-mRNAs and have

high sequence homology between each other. Consistently, our study demonstrates that gawky has a very limited binding capacity towards the host mRNAs of MRE circRNAs (Figure 1E–G; Supplementary Figure S1C-E). This fact greatly prevents the potential role of the host linear mRNAs in regulating gawky and transcription. Indeed, we confirmed that stress-induced transcription was not altered in cells stably overexpressing the linear version of MRE circRNAs during stress (Figure 2G). More importantly, the aforementioned finding also implicates that the selectivity of RNA recognition of certain RBPs does not simply depend on the nucleotide sequences. In line with the phenotype, many other RBPs (e.g. NF90/NF110, IGF2BP3 and MDM2) were reported to show a specific binding affinity towards certain circRNAs, rather than their linear isoforms (62,77,84). Given that circRNAs tend to be highly-structured, particularly under stressed conditions (76), we speculate that (i) these RBPs might employ the unique structural features of circRNAs (e.g. the distinct secondary and/or tertiary structures) to distinguish each form of transcripts, and (ii) MRE might have a role in maintaining these structures in MRE circRNAs. Extensive research with methodologies for studying the complexity and diversity of RNA–protein complexes is required to uncover the structural basis of the specific interaction, which is one of the aims in our lab currently.

Recent studies have revealed that a subgroup of *cis*-acting circRNAs are able to directly regulate Pol II activities by generating stable R-loops in proximity to the loci where they are transcribed (31,33). For example, the RNA–DNA hybrid formed by *circMLL* and the *MLL* locus can serve as a physical barrier to induce a robust transcriptional pausing, thereby blocking or slowing down the steps of Pol II elongation in the vicinity of the R-loop sites (33). However, we found that MRE circRNAs mainly localized in the cytoplasm (Figure 1I–K; Supplementary Figure S3A,B) and their Nuc/Cyto ratios were significantly reduced in response to copper stress (Figure 1L–N; Supplementary Figure S3E,F), extremely limiting their chances of R-loop formation. We also noticed that the repressive effects of MRE circRNAs were not restricted to their host genes. Instead, MRE circRNA-mediated regulation was general for hundreds of stress-inducible genes (Figures 6, 7A; Supplementary Figure S14, S15), indicating that MRE circRNAs are a class of *trans*-acting factors. More importantly, our DRIPc-qPCR analysis showed that MRE circRNAs cannot be pulled down by the R-loop-specific S9.6 antibody (Supplementary Figure S11). Therefore, we excluded the possibility that MRE circRNAs might function through an R-loop-mediated pathway. In addition, it is important to remember that certain circRNAs control transcription through specific RNA-RNA interactions with regulatory noncoding RNAs (28). This can be exemplified by two exon-intron circRNAs (*circEIF3J* and *circPAIP2*), each of which contains a U1 snRNA binding site and can enhance Pol II occupancy at its host gene through base-pairing with U1 snRNA (28). In this regard, no potential U1 snRNA binding site was found in either *circCG32369(2)* or *circMCPH1(2,3,4,5)*. Thus it is unlikely that MRE circRNAs function with U1 snRNA, at least in the case of *circCG32369(2)* and *circMCPH1(2,3,4,5)*. However, we cannot ignore the interplays between MRE circRNAs and other regulatory noncoding RNAs with known roles in transcription, such as 7SK and B2 (85,86). More investigations are needed to fill the gap.

Data availability

High-throughput sequencing data were deposited in BioProject (PRJNA1039137).

Supplementary Data

Supplementary Data are available at NAR Online.

Acknowledgements

We thank Dr Jeremy E. Wilusz (University of Pennsylvania and Baylor College of Medicine) for providing useful expression vectors. We also thank Dr Qin Deng at Analytical and Testing Center of Chongqing University for the assistance with confocal microscopy analyses.

Author contributions: C.H. conceived this project, supervised its execution and provide the major funding. R.S., M.Z., J.L. and G.S. performed experiments, analyzed data or provided the experimental material. C.H. wrote the manuscript with input from the other co-authors.

Funding

National Natural Science Foundation of China [32270601, 32070633]; Chongqing Talents Plan for Young Talents [cstc2022ycjh-bgzxm0140]; Fundamental Research Funds for the Central Universities of China [2023CDJXY-009]; Innovation Support Program for Overseas Returned Scholars of Chongqing, China [cx2019142]. Funding for open access charge: National Natural Science Foundation of China [32070633].

Conflict of interest statement

None declared.

References

1. de Nadal,E., Ammerer,G. and Posas,F. (2011) Controlling gene expression in response to stress. *Nat. Rev. Genet.*, **12**, 833–845.
2. Vihervaara,A., Duarte,F.M. and Lis,J.T. (2018) Molecular mechanisms driving transcriptional stress responses. *Nat. Rev. Genet.*, **19**, 385–397.
3. Chen,X. and Huang,C. (2023) Chromatin-interacting RNA-binding proteins regulate transcription. *Trends Cell Biol.*, **33**, 625–629.
4. Cao,J., Luo,Z., Cheng,Q., Xu,Q., Zhang,Y., Wang,F., Wu,Y. and Song,X. (2015) Three-dimensional regulation of transcription. *Protein Cell*, **6**, 241–253.
5. Hentze,M.W., Castello,A., Schwarzl,T. and Preiss,T. (2018) A brave new world of RNA-binding proteins. *Nat. Rev. Mol. Cell Biol.*, **19**, 327–341.
6. Corley,M., Burns,M.C. and Yeo,G.W. (2020) How RNA-binding proteins interact with RNA: molecules and mechanisms. *Mol. Cell*, **78**, 9–29.
7. Gebauer,F., Schwarzl,T., Valcarcel,J. and Hentze,M.W. (2021) RNA-binding proteins in human genetic disease. *Nat. Rev. Genet.*, **22**, 185–198.
8. Fischer,J.W., Busa,V.F., Shao,Y. and Leung,A.K.L. (2020) Structure-mediated RNA decay by UPF1 and G3BP1. *Mol. Cell*, **78**, 70–84.
9. Shao,W., Bi,X., Pan,Y., Gao,B., Wu,J., Yin,Y., Liu,Z., Peng,M., Zhang,W., Jiang,X., *et al.* (2022) Phase separation of RNA-binding protein promotes polymerase binding and transcription. *Nat. Chem. Biol.*, **18**, 70–80.

10. Jia,R., Lin,J., You,J., Li,S., Shan,G. and Huang,C. (2022) The DEAD-box helicase hlc regulates basal transcription and chromatin opening of stress-responsive genes. *Nucleic Acids Res.*, **50**, 9175–9189.
11. Jia,R., Song,Z., Lin,J., Li,Z., Shan,G. and Huang,C. (2021) Gawky modulates MTF-1-mediated transcription activation and metal discrimination. *Nucleic Acids Res.*, **49**, 6296–6314.
12. Ren,Y., Huo,Y., Li,W., He,M., Liu,S., Yang,J., Zhao,H., Xu,L., Guo,Y., Si,Y., *et al.* (2021) A global screening identifies chromatin-enriched RNA-binding proteins and the transcriptional regulatory activity of QKI5 during monocytic differentiation. *Genome Biol.*, **22**, 290.
13. Van Nostrand,E.L., Freese,P., Pratt,G.A., Wang,X., Wei,X., Xiao,R., Blue,S.M., Chen,J.Y., Cody,N.A.L., Dominguez,D., *et al.* (2020) A large-scale binding and functional map of human RNA-binding proteins. *Nature*, **583**, 711–719.
14. Xiao,R., Chen,J.Y., Liang,Z., Luo,D., Chen,G., Lu,Z.J., Chen,Y., Zhou,B., Li,H., Du,X., *et al.* (2019) Pervasive chromatin-RNA binding protein interactions enable RNA-based regulation of transcription. *Cell*, **178**, 107–121.
15. Xu,Y., Huangyang,P., Wang,Y., Xue,L., Devericks,E., Nguyen,H.G., Yu,X., Oses-Prieto,J.A., Burlingame,A.L., Miglani,S., *et al.* (2021) ERalpha is an RNA-binding protein sustaining tumor cell survival and drug resistance. *Cell*, **184**, 5215–5229.
16. Zhou,M., Xiao,M.S., Li,Z. and Huang,C. (2021) New progresses of circular RNA biology: from nuclear export to degradation. *RNA Biol.*, **18**, 1365–1373.
17. Kristensen,L.S., Andersen,M.S., Stagsted,L.V.W., Ebbesen,K.K., Hansen,T.B. and Kjems,J. (2019) The biogenesis, biology and characterization of circular RNAs. *Nat. Rev. Genet.*, **20**, 675–691.
18. Xiao,M.S., Ai,Y. and Wilusz,J.E. (2020) Biogenesis and functions of circular RNAs come into focus. *Trends Cell Biol.*, **30**, 226–240.
19. Chen,L.L. (2020) The expanding regulatory mechanisms and cellular functions of circular RNAs. *Nat. Rev. Mol. Cell Biol.*, **21**, 475–490.
20. Liu,C.X. and Chen,L.L. (2022) Circular RNAs: characterization, cellular roles, and applications. *Cell*, **185**, 2016–2034.
21. Chen,L., Huang,C. and Shan,G. (2022) Circular RNAs in physiology and non-immunological diseases. *Trends Biochem. Sci.*, **47**, 250–264.
22. Chen,X., Zhou,M., Yant,L. and Huang,C. (2022) Circular RNA in disease: basic properties and biomedical relevance. *Wiley Interdiscip. Rev. RNA*, **13**, e1723.
23. Li,J., Sun,D., Pu,W., Wang,J. and Peng,Y. (2020) Circular RNAs in cancer: biogenesis, function, and clinical significance. *Trends Cancer*, **6**, 319–336.
24. Zhou,M., Li,S. and Huang,C. (2024) Physiological and pathological functions of circular RNAs in the nervous system. *Neural Regen. Res.*, **19**, 342–349.
25. Yan,L. and Chen,Y.G. (2020) Circular RNAs in immune response and viral infection. *Trends Biochem. Sci.*, **45**, 1022–1034.
26. Weigelt,C.M., Sehgal,R., Tain,L.S., Cheng,J., Esser,J., Pahl,A., Dieterich,C., Gronke,S. and Partridge,L. (2020) An insulin-sensitive circular RNA that regulates lifespan in drosophila. *Mol. Cell*, **79**, 268–279.
27. Song,Z., Lin,J., Su,R., Ji,Y., Jia,R., Li,S., Shan,G. and Huang,C. (2022) eIF3j inhibits translation of a subset of circular RNAs in eukaryotic cells. *Nucleic Acids Res.*, **50**, 11529–11549.
28. Li,Z., Huang,C., Bao,C., Chen,L., Lin,M., Wang,X., Zhong,G., Yu,B., Hu,W., Dai,L., *et al.* (2015) Exon-intron circular RNAs regulate transcription in the nucleus. *Nat. Struct. Mol. Biol.*, **22**, 256–264.
29. Stoll,L., Rodriguez-Trejo,A., Guay,C., Brozzi,F., Bayazit,M.B., Gattesco,S., Menoud,V., Sobel,J., Marques,A.C., Veno,M.T., *et al.* (2020) A circular RNA generated from an intron of the insulin gene controls insulin secretion. *Nat. Commun.*, **11**, 5611.
30. Conn,V.M., Hugouvieux,V., Nayak,A., Conos,S.A., Capovilla,G., Cildir,G., Jourdain,A., Tergaonkar,V., Schmid,M., Zubieta,C., *et al.* (2017) A circRNA from SEPALLATA3 regulates splicing of its cognate mRNA through R-loop formation. *Nat. Plants*, **3**, 17053.
31. Xu,X., Zhang,J., Tian,Y., Gao,Y., Dong,X., Chen,W., Yuan,X., Yin,W., Xu,J., Chen,K., *et al.* (2020) CircRNA inhibits DNA damage repair by interacting with host gene. *Mol. Cancer*, **19**, 128.
32. Liu,Y., Su,H., Zhang,J., Liu,Y., Feng,C. and Han,F. (2020) Back-spliced RNA from retrotransposon binds to centromere and regulates centromeric chromatin loops in maize. *PLoS Biol.*, **18**, e3000582.
33. Conn,V.M., Gabryelska,M., Toubia,J., Kirk,K., Gantley,L., Powell,J.A., Cildir,G., Marri,S., Liu,R., Stringer,B.W., *et al.* (2023) Circular RNAs drive oncogenic chromosomal translocations within the MLL recombinome in leukemia. *Cancer Cell*, **41**, 1309–1326.
34. Enuka,Y., Lauriola,M., Feldman,M.E., Sas-Chen,A., Ulitsky,I. and Yarden,Y. (2016) Circular RNAs are long-lived and display only minimal early alterations in response to a growth factor. *Nucleic Acids Res.*, **44**, 1370–1383.
35. Jia,R., Xiao,M.S., Li,Z., Shan,G. and Huang,C. (2019) Defining an evolutionarily conserved role of GW182 in circular RNA degradation. *Cell Discov.*, **5**, 45.
36. Liang,D., Tatomer,D.C., Luo,Z., Wu,H., Yang,L., Chen,L.L., Cherry,S. and Wilusz,J.E. (2017) The output of protein-coding genes shifts to circular RNAs when the pre-mRNA processing machinery is limiting. *Mol. Cell*, **68**, 940–954.
37. Kramer,M.C., Liang,D., Tatomer,D.C., Gold,B., March,Z.M., Cherry,S. and Wilusz,J.E. (2015) Combinatorial control of Drosophila circular RNA expression by intronic repeats, hnRNPs, and SR proteins. *Genes Dev.*, **29**, 2168–2182.
38. You,J., Song,Z., Lin,J., Jia,R., Xia,F., Li,Z. and Huang,C. (2021) RNAi-directed knockdown induces nascent transcript degradation and premature transcription termination in the nucleus. *Cell Discov.*, **7**, 79.
39. Chen,L., Wang,Y., Lin,J., Song,Z., Wang,Q., Zhao,W., Wang,Y., Xiu,X., Deng,Y., Li,X., *et al.* (2022) Exportin 4 depletion leads to nuclear accumulation of a subset of circular RNAs. *Nat. Commun.*, **13**, 5769.
40. Sanz,L.A. and Chédin,F. (2019) High-resolution, strand-specific R-loop mapping via S9.6-based DNA–RNA immunoprecipitation and high-throughput sequencing. *Nat. Protoc.*, **14**, 1734–1755.
41. Huang,C., Wang,X., Liu,X., Cao,S. and Shan,G. (2015) RNAi pathway participates in chromosome segregation in mammalian cells. *Cell Discov.*, **1**, 15029.
42. Song,Z., Jia,R., Tang,M., Xia,F., Xu,H., Li,Z. and Huang,C. (2021) Antisense oligonucleotide technology can be used to investigate a circular but not linear RNA-mediated function for its encoded gene locus. *Sci. China Life Sci.*, **64**, 784–794.
43. Bolger,A.M., Lohse,M. and Usadel,B. (2014) Trimmomatic: a flexible trimmer for Illumina sequence data. *Bioinformatics*, **30**, 2114–2120.
44. Dobin,A., Davis,C.A., Schlesinger,F., Drenkow,J., Zaleski,C., Jha,S., Batut,P., Chaisson,M. and Gingeras,T.R. (2013) STAR: ultrafast universal RNA-seq aligner. *Bioinformatics*, **29**, 15–21.
45. Liao,Y., Smyth,G.K. and Shi,W. (2014) featureCounts: an efficient general purpose program for assigning sequence reads to genomic features. *Bioinformatics*, **30**, 923–930.
46. Love,M.I., Huber,W. and Anders,S. (2014) Moderated estimation of fold change and dispersion for RNA-seq data with DESeq2. *Genome Biol.*, **15**, 550.
47. Ramírez,F., Ryan,D.P., Grüning,B., Bhardwaj,V., Kilpert,F., Richter,A.S., Heyne,S., Dündar,F. and Manke,T. (2016) deepTools2: a next generation web server for deep-sequencing data analysis. *Nucleic Acids Res.*, **44**, W160–W165.
48. Robinson,J.T., Thorvaldsdóttir,H., Winckler,W., Guttman,M., Lander,E.S., Getz,G. and Mesirov,J.P. (2011) Integrative genomics viewer. *Nat. Biotechnol.*, **29**, 24–26.
49. Yu,G.C., Wang,L.G., Han,Y.Y. and He,Q.Y. (2012) clusterProfiler: an R package for comparing biological themes among gene clusters. *OMICS*, **16**, 284–287.

50. Zhang,X.O., Dong,R., Zhang,Y., Zhang,J.L., Luo,Z., Zhang,J., Chen,L.L. and Yang,L. (2016) Diverse alternative back-splicing and alternative splicing landscape of circular RNAs. *Genome Res.*, **26**, 1277–1287.
51. Dong,X., Chen,K., Chen,W.B., Wang,J., Chang,L.P., Deng,J., Wei,L., Han,L., Huang,C.H. and He,C.J. (2022) circRIP: an accurate tool for identifying circRNA-RBP interactions. *Brief. Bioinf.*, **23**, bbac186.
52. Langmead,B., Wilks,C., Antonescu,V. and Charles,R. (2019) Scaling read aligners to hundreds of threads on general-purpose processors. *Bioinformatics*, **35**, 421–432.
53. Li,H., Handsaker,B., Wysoker,A., Fennell,T., Ruan,J., Homer,N., Marth,G., Abecasis,G., Durbin,R. and Proc,G.P.D. (2009) The sequence alignment/map format and SAMtools. *Bioinformatics*, **25**, 2078–2079.
54. Alarcon,C.R., Goodarzi,H., Lee,H., Liu,X., Tavazoie,S. and Tavazoie,S.F. (2015) HNRNPA2B1 is a mediator of m(6)A-dependent nuclear RNA processing events. *Cell*, **162**, 1299–1308.
55. Taylor,S.R., Santpere,G., Weinreb,A., Barrett,A., Reilly,M.B., Xu,C., Varol,E., Oikonomou,P., Glenwinkel,L., McWhirter,R., *et al.* (2021) Molecular topography of an entire nervous system. *Cell*, **184**, 4329–4347.
56. Robinson,M.D., McCarthy,D.J. and Smyth,G.K. (2010) edgeR: a bioconductor package for differential expression analysis of digital gene expression data. *Bioinformatics*, **26**, 139–140.
57. Chen,C.J., Chen,H., Zhang,Y., Thomas,H.R., Frank,M.H., He,Y.H. and Xia,R. (2020) TBtools: an integrative toolkit developed for interactive analyses of big biological data. *Mol. Plant*, **13**, 1194–1202.
58. Tang,D., Chen,M., Huang,X., Zhang,G., Zeng,L., Zhang,G., Wu,S. and Wang,Y. (2023) SRplot: a free online platform for data visualization and graphing. *PLoS One*, **18**, e0294236.
59. Gunther,V., Lindert,U. and Schaffner,W. (2012) The taste of heavy metals: gene regulation by MTF-1. *Biochim. Biophys. Acta*, **1823**, 1416–1425.
60. Sims,H.I., Chirn,G.W. and Marr,M.T. 2nd. (2012) Single nucleotide in the MTF-1 binding site can determine metal-specific transcription activation. *Proc. Natl. Acad. Sci. U.S.A.*, **109**, 16516–16521.
61. Chen,G., Shi,Y., Liu,M. and Sun,J. (2018) circHIPK3 regulates cell proliferation and migration by sponging miR-124 and regulating AQP3 expression in hepatocellular carcinoma. *Cell Death. Dis.*, **9**, 175.
62. Li,K., Guo,J., Ming,Y., Chen,S., Zhang,T., Ma,H., Fu,X., Wang,J., Liu,W. and Peng,Y. (2023) A circular RNA activated by TGFbeta promotes tumor metastasis through enhancing IGF2BP3-mediated PDPN mRNA stability. *Nat. Commun.*, **14**, 6876.
63. Chen,R.X., Chen,X., Xia,L.P., Zhang,J.X., Pan,Z.Z., Ma,X.D., Han,K., Chen,J.W., Judde,J.G., Deas,O., *et al.* (2019) N(6)-methyladenosine modification of circNSUN2 facilitates cytoplasmic export and stabilizes HMGA2 to promote colorectal liver metastasis. *Nat. Commun.*, **10**, 4695.
64. Haberle,V. and Stark,A. (2018) Eukaryotic core promoters and the functional basis of transcription initiation. *Nat. Rev. Mol. Cell Biol.*, **19**, 621–637.
65. Andersson,R. and Sandelin,A. (2020) Determinants of enhancer and promoter activities of regulatory elements. *Nat. Rev. Genet.*, **21**, 71–87.
66. Huang,C., Liang,D., Tatomer,D.C. and Wilusz,J.E. (2018) A length-dependent evolutionarily conserved pathway controls nuclear export of circular RNAs. *Genes Dev.*, **32**, 639–644.
67. Gaetke,L.M. and Chow,C.K. (2003) Copper toxicity, oxidative stress, and antioxidant nutrients. *Toxicology*, **189**, 147–163.
68. Kardos,J., Heja,L., Simon,A., Jablonkai,I., Kovacs,R. and Jemnitz,K. (2018) Copper signalling: causes and consequences. *Cell Commun. Signal.*, **16**, 71.
69. Guo,H., Wang,Y., Cui,H., Ouyang,Y., Yang,T., Liu,C., Liu,X., Zhu,Y. and Deng,H. (2022) Copper induces spleen damage through modulation of oxidative stress, apoptosis, DNA damage, and inflammation. *Biol. Trace Elem. Res.*, **200**, 669–677.
70. Chen,X., Cai,Q., Liang,R., Zhang,D., Liu,X., Zhang,M., Xiong,Y., Xu,M., Liu,Q., Li,P., *et al.* (2023) Copper homeostasis and copper-induced cell death in the pathogenesis of cardiovascular disease and therapeutic strategies. *Cell Death. Dis.*, **14**, 105.
71. Burke,R. (2022) Molecular physiology of copper in drosophila melanogaster. *Curr. Opin. Insect. Sci.*, **51**, 100892.
72. Harpprecht,L., Baldi,S., Schauer,T., Schmidt,A., Bange,T., Robles,M.S., Kremmer,E., Imhof,A. and Becker,P.B. (2019) A Drosophila cell-free system that senses DNA breaks and triggers phosphorylation signalling. *Nucleic Acids Res.*, **47**, 7444–7459.
73. Baldi,S. and Becker,P.B. (2013) The variant histone H2A.V of Drosophila–three roles, two guises. *Chromosoma*, **122**, 245–258.
74. Rehwinkel,J., Behm-Ansmant,I., Gatfield,D. and Izaurralde,E. (2005) A crucial role for GW182 and the DCP1:DCP2 decapping complex in miRNA-mediated gene silencing. *RNA*, **11**, 1640–1647.
75. Zander,G., Hackmann,A., Bender,L., Becker,D., Lingner,T., Salinas,G. and Krebber,H. (2016) mRNA quality control is bypassed for immediate export of stress-responsive transcripts. *Nature*, **540**, 593–596.
76. Liu,C.X., Li,X., Nan,F., Jiang,S., Gao,X., Guo,S.K., Xue,W., Cui,Y., Dong,K., Ding,H., *et al.* (2019) Structure and degradation of circular RNAs regulate PKR activation in innate immunity. *Cell*, **177**, 865–880.
77. Li,X., Liu,C.X., Xue,W., Zhang,Y., Jiang,S., Yin,Q.F., Wei,J., Yao,R.W., Yang,L. and Chen,L.L. (2017) Coordinated circRNA biogenesis and function with NF90/NF110 in viral infection. *Mol. Cell*, **67**, 214–227.
78. Armakola,M., Higgins,M.J., Figley,M.D., Barmada,S.J., Scarborough,E.A., Diaz,Z., Fang,X., Shorter,J., Krogan,N.J., Finkbeiner,S., *et al.* (2012) Inhibition of RNA lariat debranching enzyme suppresses TDP-43 toxicity in ALS disease models. *Nat. Genet.*, **44**, 1302–1309.
79. Wisniewski,J.R., Hein,M.Y., Cox,J. and Mann,M. (2014) A "proteomic ruler" for protein copy number and concentration estimation without spike-in standards. *Mol. Cell. Proteomics*, **13**, 3497–3506.
80. Tyanova,S., Temu,T., Sinitcyn,P., Carlson,A., Hein,M.Y., Geiger,T., Mann,M. and Cox,J. (2016) The Perseus computational platform for comprehensive analysis of (prote)omics data. *Nat. Methods*, **13**, 731–740.
81. Rey,G., Milev,N.B., Valekunja,U.K., Ch,R., Ray,S., Silva Dos Santos,M., Nagy,A.D., Antrobus,R., MacRae,J.I. and Reddy,A.B. (2018) Metabolic oscillations on the circadian time scale in Drosophila cells lacking clock genes. *Mol. Syst. Biol.*, **14**, e8376.
82. Abdelmohsen,K., Panda,A.C., Munk,R., Grammatikakis,I., Dudekula,D.B., De,S., Kim,J., Noh,J.H., Kim,K.M., Martindale,J.L., *et al.* (2017) Identification of HuR target circular RNAs uncovers suppression of PABPN1 translation by CircPABPN1. *RNA Biol.*, **14**, 361–369.
83. Bronisz,A., Rooj,A.K., Krawczynski,K., Peruzzi,P., Salinska,E., Nakano,I., Purow,B., Chiocca,E.A. and Godlewski,J. (2020) The nuclear DICER-circular RNA complex drives the deregulation of the glioblastoma cell microRNAome. *Sci. Adv.*, **6**, eabc0221.
84. Du,W.W., Fang,L., Yang,W., Wu,N., Awan,F.M., Yang,Z. and Yang,B.B. (2017) Induction of tumor apoptosis through a circular RNA enhancing Foxo3 activity. *Cell Death Differ.*, **24**, 357–370.
85. Espinoza,C.A., Allen,T.A., Hieb,A.R., Kugel,J.F. and Goodrich,J.A. (2004) B2 RNA binds directly to RNA polymerase II to repress transcript synthesis. *Nat. Struct. Mol. Biol.*, **11**, 822–829.
86. Yang,Z., Zhu,Q., Luo,K. and Zhou,Q. (2001) The 7SK small nuclear RNA inhibits the CDK9/cyclin T1 kinase to control transcription. *Nature*, **414**, 317–322.

Received: November 22, 2023. **Revised:** February 14, 2024. **Editorial Decision:** February 18, 2024. **Accepted:** February 20, 2024